Journal of Power Sources 195 (2010) 4531–4553

Contents lists available at ScienceDirect

Journal of Power Sources

journal homepage: www.elsevier.com/locate/jpowsour

Review

A critical review of two-phase flow in gas flow channels of proton exchange membrane fuel cells

Ryan Anderson[a,b], Lifeng Zhang[a,b], Yulong Ding[a,b], Mauricio Blanco[a,b], Xiaotao Bi[a,b,*], David P. Wilkinson[a,b,*]

[a] Department of Chemical and Biological Engineering, University of British Columbia, 2360 East Mall, Vancouver, BC, Canada V6T 1Z3
[b] Clean Energy Research Centre, 2360 East Mall, Vancouver, BC, Canada V6T 1Z3

ARTICLE INFO

Article history:
Received 29 October 2009
Received in revised form
25 December 2009
Accepted 29 December 2009
Available online 13 January 2010

Keywords:
PEM fuel cell
Two-phase flow
Water management
CFD simulation
Flow channels

ABSTRACT

Water management in PEM fuel cells has received extensive attention due to its key role in fuel cell performance. The unavoidable water, from humidified gas streams and electrochemical reaction, leads to gas–liquid two-phase flow in the flow channels of fuel cells. The presence of two-phase flow increases the complexity in water management in PEM fuel cells, which remains a challenging hurdle in the commercialization of this technology. Unique water emergence from the gas diffusion layer, which is different from conventional gas–liquid two-phase flow where water is introduced from the inlet together with the gas, leads to different gas–liquid flow behaviors, including pressure drop, flow pattern, and liquid holdup along flow field channels. These parameters are critical in flow field design and fuel cell operation and therefore two-phase flow has received increasing attention in recent years. This review emphasizes gas–liquid two-phase flow in minichannels or microchannels related to PEM fuel cell applications. In situ and ex situ experimental setups have been utilized to visualize and quantify two-phase flow phenomena in terms of flow regime maps, flow maldistribution, and pressure drop measurements. Work should continue to make the results more relevant for operating PEM fuel cells. Numerical simulations have progressed greatly, but conditions relevant to the length scales and time scales experienced by an operating fuel cell have not been realized. Several mitigation strategies exist to deal with two-phase flow, but often at the expense of overall cell performance due to parasitic power losses. Thus, experimentation and simulation must continue to progress in order to develop a full understanding of two-phase flow phenomena so that meaningful mitigation strategies can be implemented.

Contents

* Corresponding authors. Tel.: +1 604 8224888; fax: +1 604 8226003.
E-mail addresses: xbi@chbe.ubc.ca (X. Bi), dwilkinson@chbe.ubc.ca (D.P. Wilkinson).

0378-7753/$ – see front matter © 2010 Elsevier B.V. All rights reserved.
doi:10.1016/j.jpowsour.2009.12.123

Nomenclature

A	area (cm^2)
A	advancing contact angle (°)
Bo	Bond number
F	Faraday's constant (96,485.339 C mol^{-1})
F_x	Force from contribution x (N)
g	gravity ($m\,s^{-2}$)
I	current (A)
i	current density ($A\,cm^{-2}$)
L	characteristic length (m)
M	molecular weight ($g\,mol^{-1}$)
m	molar flow rate ($mol\,s^{-1}$)
R	receding contact angle
Su	Suratman number
u	superficial velocity ($m\,s^{-1}$)
ΔP	pressure drop (kPa)

Greek letters

α	water transfer coefficient
ρ	density ($g\,cm^{-3}$)
μ	viscosity (Pa s)
λ	stoichiometric ratio
γ	surface tension ($N\,m^{-1}$)
θ	contact angle (°)
α	half-angle (°)
β	inclination angle (°)

Subscripts and superscripts

$O_{2,need}$	required oxygen demand at a given current density
act	active
g	gas phase
l	liquid phase
P	pressure

1. Introduction

The proton exchange membrane (PEM) fuel cell has received much attention in recent decades as a clean and efficient way to generate power for various applications due to its high energy efficiency, low operating temperature, and low to zero emissions during its operation. In particular, it has been considered one of the most promising alternatives to fossil-based fuel engines for automotive applications. The electrochemical reaction between hydrogen fuel and oxygen oxidant produces electricity, with the only emissions being excess heat and water. The PEM fuel cell is thus an environmentally viable option that is also capable of achieving high power density and high efficiency.

However, several technical issues still exist that impede the further use of fuel cells in practical applications. One major issue that has received a great deal of attention is proper water management in the fuel cell. This issue is particularly important because too little water will cause membrane dehydration, which limits proton conductivity, and too much water can flood the fuel cell, causing less reactant to reach active catalyst sites and consequently decreasing the cell performance. A recent review [1] detailed issues associated with water management, which described the role of each layer of the PEM fuel cell 'sandwich' and how each area is prone to flooding. The paper also detailed mitigation strategies based on (1) engineering principles and changing operating conditions and (2) modification of materials. While comprehensive in the overall picture of water management, little emphasis is placed on gas–liquid two-phase flow issues in the flow field channel itself. Trabold [2] noted the importance of two-phase flow research in PEM fuel cells, and explained that the gas–liquid flow within the flow channels is complex and requires an understanding of electrochemistry, heat and mass transfer, and fluid mechanics. Knowing the air and liquid velocities in the channel allows one to develop flow regime maps, which have been studied in two-phase flow research. Different operating conditions can lead to different flow patterns though, which can lead to flow maldistribution among multiple channels to satisfy the equal pressure drop between a single inlet and outlet of the manifold. Thus, many competing variables are noted in PEM fuel cell two-phase flow.

In addition to experimental efforts, many attempts have been made to model and simulate the two-phase transport phenomena in PEM fuel cells. In particular, computational fluid dynamics (CFD) is considered to be a very powerful tool in fuel cell design and operation optimization. In the literature, the earliest PEM fuel cell models date back to the early 1990s by Springer et al. [3] and Bernardi and Verbrugge [4]. Increasingly complex and detailed models have been developed since, from one-dimensional, single-phase flow, isothermal, steady-state and single layer models to three-dimensional, two-phase flow, non-isothermal, transient and multiple layer models. However, due to the various complicated phenomena in PEM fuel cells, the modeling and simulation of PEM fuel cells still remains a challenge. Complications include two-phase flow, electrochemical reaction, charge transport, diffusion in porous media, and coupling different length scales (such as the nanometer components of catalysts, the micrometer heterogeneous pores in the gas diffusion layers (GDLs), and the millimeter dimensions of flow field channels). To our knowledge, there has not

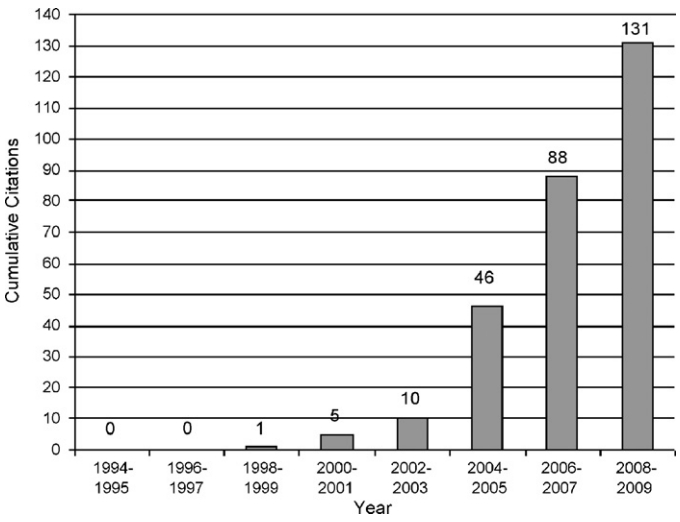

Fig. 1. Cumulative number of papers published for keywords: "two-phase flow" and "PEM fuel cells" since 1994.

been a comprehensive review of PEM fuel cell models focusing on numerical simulations of two-phase flow in flow field channels of PEM fuel cells, including droplet behaviors, flow field maldistribution, and channel design strategies for the mitigation of flooding.

This paper aims to present an up-to-date review on two-phase flow in PEM fuel cell flow channels. A thorough review is important now as the number of papers published related specifically to two-phase flow and PEM fuel cells continues to increase, which is shown in Fig. 1.

This review emphasizes gas–liquid two-phase flow in minichannels or microchannels ($D_{\text{microchannel}} < 1$ mm) related to PEM fuel cell applications. The focus is on PEM fuel cells under normal operating conditions (ambient temperature to 100 °C operation), with two-phase flow issues related to startup or shutdown neglected. The experimental approaches and results of researchers in both active fuel cells (in situ) and in channels designed to mimic operational fuel cells (ex situ) are considered. CFD simulations of two-phase flow in PEM fuel cell channels are also described in detail for in situ and ex situ approaches. Mitigation strategies specific to water flooding in channels are also presented.

2. Experimental visualization techniques

This section reviews techniques for detecting water in minichannels, focusing on direct optical visualization while referencing other methods reported in the literature. A discussion of the uses and the results of these techniques in active fuel cells are given in Section 3.

2.1. Optical visualization

The most common technique to observe flow field flooding is to use a transparent fuel cell. A typical schematic diagram of a transparent fuel cell is shown in Fig. 2.

The membrane electrode assembly (MEA) is sandwiched between flow field plates and transparent end plates for viewing. Not shown are the means to collect current, plates for heating (either electrically or via cooling water), or compression plates since these are common to all fuel cells and are not novel in regards to a transparent fuel cell. Machining the flow field directly into a metal plate allows the flow field plate to also act as the current collector. In Fig. 2, gas enters via port 1 and exits via port 2. The manifolds (labeled 3) distribute the gas to the flow channels (labeled 4). The flow field plates in this schematic are symmetrical about the

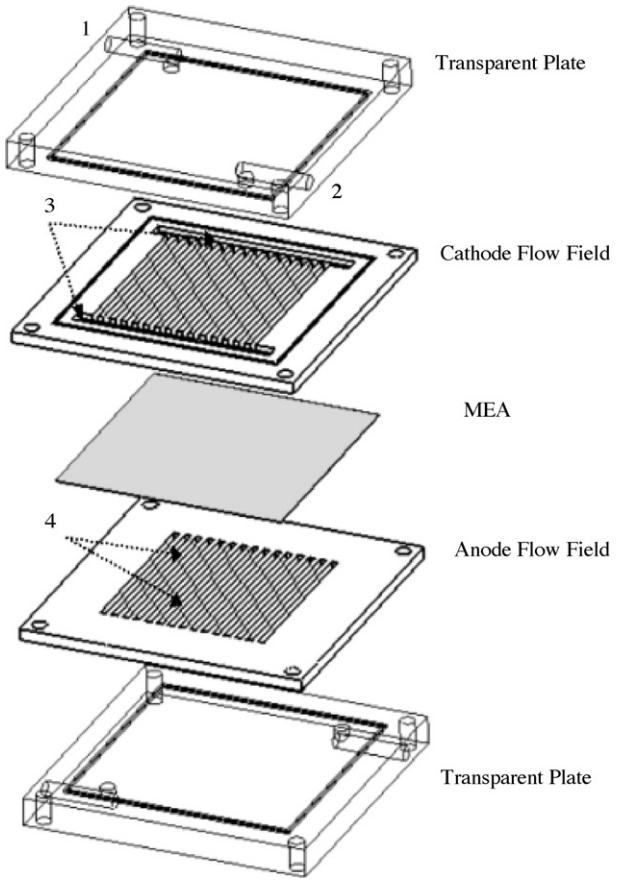

Fig. 2. Schematic of a typical transparent PEM fuel cell.

MEA. This design is not the only means of creating a transparent cell but contains the components commonly found in the literature. Different phenomena to be studied lead to specific designs for a transparent fuel cell, and Table 1 summarizes the designs of several research groups, including relevant channel dimensions, materials, and flow field design.

Tüber et al. [9] conducted a highly cited work on transparent fuel cells. A steel rib was placed between an MEA and a Plexiglas end plate, with the rib defining the depth and the landing width of two channels. Gas was introduced from the Plexiglas above via one common inlet hole. The unit was compressed with screws and a copper wire was attached to the rib for current collection. As shown in Table 1, metals are often used for flow field plates. Weng et al. [11] showed that a brass plate could be used for the anode and cathode flow fields with extension areas included for electric heating or convective cooling. Clear acrylic plates acted as end plates on the cathode and anode side, allowing for visualization of either side of the cell. Stainless steel is a common flow field material in transparent cells [5,6,8,9,12,13,19], and the plates are often gold plated to avoid corrosion and to increase conductivity. When clear acrylic end plates are used they are prone to fogging, and it can be difficult to discern between liquid water emerging into the channels and liquid water condensing on the clear plate. One solution to this problem is to use an antifogging coating [5], though this solution causes the clear polycarbonate plate to be very hydrophilic, which is not representative of commercially used graphite flow field plates that are hydrophobic. Another interesting choice for an optical plate is zinc selenide, as used by Hakenjos et al. [10]. Zinc selenide is transparent to optical light for direct visualization and IR irradiations for the determination of the temperature distribution with an IR camera. A barium fluoride plate is also transparent

Table 1
Transparent fuel cell designs.

Author	Flow field type	Flow field material	Channel dimensions ($l \times w \times d$)	Transparent plate material
Zhang et al. [5]	7 parallel channels	Gold coated stainless steel	100 mm × 1 mm × 0.5 mm Active area = 14 cm^2	Antifogging coated polycarbonate
Liu et al. [6]	9 parallel channels (vertical orientation)	Gold coated stainless steel	22.4 mm × 0.8 mm × 1 mm	Plexiglas
Ous and Arcoumanis [7]	13 serpentine channels	Graphite	655 mm × 1.5 mm × 1.5 mm	Plexiglas
Masuda et al. [8]	Single straight channel	Gold coated stainless steel	30 mm × 1.6 mm × 1 mm	Glass
Tüber et al. [9]	2 parallel channels	Stainless steel	50 mm × 1.5 mm × 1 mm	Plexiglass
Hakenjos et al. [10]	Single serpentine	Graphite	1 mm × 1 mm ($w \times d$) Active area = 20.25 cm^2	Zinc Selenide
Weng et al. [11]	Two serpentine channels	Brass	2 mm × 2 mm ($w \times d$) Active area = 10 cm^2	Acrylic
Spernjak et al. [12]	Single serpentine	Stainless steel 316	0.8 mm × 1 mm ($w \times d$) Active area = 10 cm^2	Polycarbonate
Ge and Wang [13]	(a) 7 parallel channels (b) 4 serpentine channels	Gold plated stainless steel	(a) 1 mm × 0.5 mm ($w \times d$) Active area = 14 cm^2 (b) 70 mm × 1 mm × 0.5 mm Active area = 5 cm^2	Polycarbonate
Theodorakakos et al. [14]	Single serpentine	Plexiglas	1.46 mm × 0.28 mm ($w \times d$)	Plexiglas
Shimoi et al. [15]	3 parallel channels	Brass	100 mm × 3 mm × 1 mm	Sapphire (Al_2O_3)
Kim et al. [16]	35 serpentine channels	Carbon	0.7 mm × 1 mm ($w \times d$) Active area = 25 cm^2	Acrylic
Sugiura et al. [17]	Single serpentine 14 parallel	–	1.6 × 0.8 mm ($w \times d$) Active area = 25 cm^2	Polycarbonate
Ma et al. [18]	Single straight channel	Graphite	125 mm × 1.5 mm × 1 mm Active area = 5 cm^2	
Yang et al. [19]	7 parallel channels	Gold coated stainless steel	100 mm × 1 mm × 1 mm Active area = 14 cm^2	Polycarbonate

to IR light and can be used to determine temperature distributions [20].

One drawback of transparent cells is the lack of quantitative information provided. Viewing the channel from the top does not offer depth resolution, and the true volume of films, slugs, and droplets in the channel cannot be analyzed. The reflective GDL background also complicates image processing [12]. The images are often usefully correlated with pressure or voltage data, but this correlation provides only qualitative details about the cell [21]. The subjective nature of these qualitative correlations makes it difficult to standardize between authors. Another issue associated with transparent cells is the material of construction. The view material is typically an insulator and heat transfer of the fuel cell can be modified. Therefore, the results do not reproduce the real cell behavior. In addition, the surface properties are very important in analyzing two-phase flow, especially contact angles, and little consideration is given to this problem in the literature. For instance, specific results found in a cell with a Plexiglas end plate may differ from the results found in a cell using traditional graphite plates. Since transparent cells define flow channels with an optical plate top, flow field plate walls, and a GDL bottom, three contact angles must be considered when analyzing the surface properties and droplet dynamics. Another potentially important parameter is the surface roughness of the flow field plates. Despite these drawbacks, visualization cells provide a method to validate existing models and to further understand the influence of key operating variables. As pointed out by Chang et al. [22], this validation is particularly important in incorporating two-phase flow into existing models. Coupling the optical visualization with other techniques to monitor liquid water also enhances the use of transparent cells [23].

2.2. Other visualization systems

Other methods to visualize two-phase flow include neutron radiography and magnetic resonance imaging (MRI). Neutron radiography can be used to obtain 2D images of liquid water [24,25]. This technique allows the user to gain greater quantitative information. In an MRI system, Dunbar and Masel [26] attempted to mimic actual materials used in typical flow fields. Ferromagnetic materials like iron or nickel are unsuitable due to the magnetic field, so Teflon® flow fields coated with a graphite layer (Aquadag) to represent the hydrophobicity of commercially available graphite flow fields were used to avoid complications in the MRI. Recent reviews of water visualization and measurements by these methods and others have been discussed in greater detail [23,27]. These methods help validate the qualitative information derived from optical visualization cells, and also help validate the results of numerical models.

3. In situ experimental two-phase flow studies in PEM fuel cells

In active PEM fuel cells, the presence of liquid water has been observed by the visualization techniques described in Section 2. This section describes two-phase flow studies in operational PEM fuel cells, which is an important distinction because two-phase flow in fuel cells is different from traditional two-phase flow in other applications [28]. One such difference is that water content changes along the length of the channel as water is introduced to the channels from the GDL after reaction at the catalyst surface. This introduction method means water droplet generation and removal at the GDL surface into the channel must be considered. This issue is further complicated by the randomness of the location of the emerging droplet because the removal process depends on whether the droplet is created on the GDL surface towards the center or the wall of the channel [7]. The surfaces of the channel also have dissimilar contact angles, since the transparent plates, flow field plates, and the GDLs have different contact angles, which influences droplet behavior. A schematic showing these three surfaces is shown in Fig. 3.

Once the droplet is removed from the GDL surface, it can coalesce with droplets downstream, changing the behavior of the

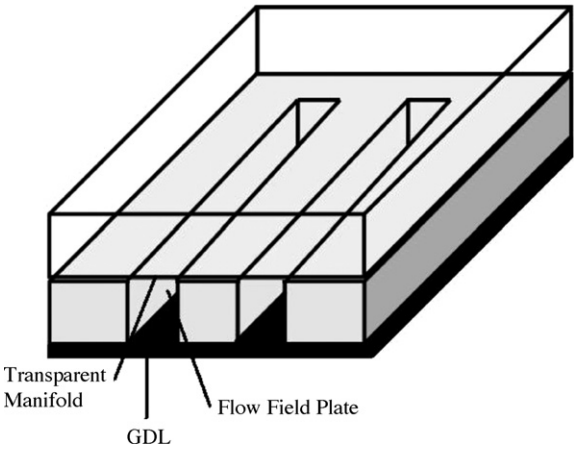

Fig. 3. Schematic of channel surfaces in a transparent fuel cell.

two-phase flow. Also, the two-phase flow in fuel cell flow channels is characterized by a large gas to liquid flow ratio and a decreasing mole fraction of the reactant gas down the length of the channel due to consumption. Non-uniform temperature distributions created by local hotspots can also change the amount of water that will remain in the gas phase, which affects the water balance in the flow channel [20]. Non-uniform current distribution, which changes the amount of water being produced, can also lead to non-uniform distribution of the water product in the channels.

3.1. Gas channel two-phase flow: causes and problems

Liquid water is transported in the fuel cell by various mechanisms, and a review of the PEM fuel cell water balance has recently been published [29]. Water can condense in the flow field channel from the inlet gas due to decreased operating temperature, increased pressure, or increased gas humidification if the saturation vapor pressure is reached. Electroosmotic drag carries water from the anode to the cathode via protons moving through the electrolyte. Back diffusion occurs when the product water establishes a concentration gradient between the cathode and anode, causing water to diffuse towards the anode. The product water must then diffuse through the GDL to reach the flow field channels. Once liquid water enters the channels, several problems can emerge, and major issues associated with gas channel flooding include [28]:

- Blockage of the channel by liquid water, which can increase the pressure drop in the channel.
- Non-uniform current distribution and reactant distribution.
- Blockage of reactant gas transport to the active reaction sites due to the formation of a liquid film on the GDL surface.

3.2. Flow patterns

In an operating fuel cell, two-phase flow patterns impact the pressure drop and liquid water distribution in the flow channel, which will alter the PEM fuel cell performance. Liquid water holdup is a particular concern for low Bond number ($10^{-4} \leq Bo \leq 10^{-1}$) and low Suratman number ($10^3 \leq Su \leq 10^5$) environments [6]. The Bond number is the ratio of gravitational force (body force) to surface tension for a liquid surface and the Suratman number is the ratio of surface tension to viscous forces. The equations for these dimensionless groups are shown below:

$$Bo = \frac{\rho g L^2}{\gamma} \tag{1}$$

$$Su = \frac{\gamma \rho L}{\mu^2} \tag{2}$$

where ρ is the density difference between phases, g is the acceleration due to gravity, L is a characteristic length such as the drop radius, γ is the surface tension, and μ is the dynamic viscosity. For low *Bo* and low *Su* conditions, the noted flow patterns are slug flow, core-annular, and transition flows [6]. Typical flow patterns in operating fuel cells can be seen in Fig. 4 from the work of Hussaini and Wang [30].

Not all two-phase flow studies show the same flow patterns and the lack of consistency highlights the difficulty in understanding and characterizing two-phase flow in operational cells. Additionally, the schematic in Fig. 4 contains stray droplets in the description of single-phase flow, which would be more accurately described as mist flow (if enough stray droplets are noted) or as a pseudo-homogenous flow. Mist flow has been identified in an operating fuel cell but at an air stoichiometry of 10, which may be unrealistic for a fuel cell due to high parasitic power losses [5]. Further complicating the identification of flow patterns, fuel cells operate at different relative humidities and temperatures (affecting water uptake capacity), with different flow channel configurations, different flow rates, and different surfaces (GDL and channel). Individual results are thus noted for specific setups, and no work has been done to determine the effect of such operating conditions on two-phase flow in a general sense.

Flow pattern maps are useful because it shows how superficial air and liquid velocities can be exploited to give a particular flow regime. Hussaini and Wang [30] constructed a flow map showing different regions at different superficial gas and liquid velocities.

Trabold [2] recommends operating the channels in the annular flow regime, which would require a superficial gas velocity of 5–6 m s^{-1}. This regime allows water to be removed on the channel walls while leaving the GDL surface available for gas transport. To maintain this regime, though, specific operating conditions would have to be met at a given current density and stoichiometry. In flow field channels, operating gas flow rates are usually determined by the necessary stoichiometric amount of gas reactant for a designated current density (from Faraday's law) multiplied by the gas stoichiometric ratio, λ, which is defined as follows:

$$\lambda = \frac{m_{O_{2,\text{inlet}}}}{m_{O_{2,\text{need}}}} \tag{3}$$

$$m_{O_{2,\text{need}}} = \frac{I}{4F} = \frac{iA_{\text{act}}}{4F} \tag{4}$$

where $m_{O_2,\text{inlet}}$ is the number of moles of oxygen at the inlet and $m_{O_2,\text{need}}$ is the theoretical value of oxygen needed based on the current density and active surface area of MEA. In practical systems, the parasitic load or energy required for gas delivery is directly related to the pressure, volume flow rate, and pressure drop. It is therefore desirable to keep the stoichiometric ratio as low as possible while sufficiently high for effective water management [31]. Also, the GDL, flow field, and operating conditions can shift the transitions between flow regimes. The results presented in Fig. 5 are valid for that specific experimental setup only, so multiple factors in addition to superficial velocities have to be understood in order to operate the fuel cell in the desired flow regime.

3.3. Pressure drop (characteristics under active cell operating conditions)

The pressure drop is considered to be an indicator of liquid water build-up in flow field channels of a PEM fuel cell. The pressure drop increases with current density, which is usually explained by the higher reactant flow rates and higher water production rates in accordance with Faraday's law. Higher water production can mean

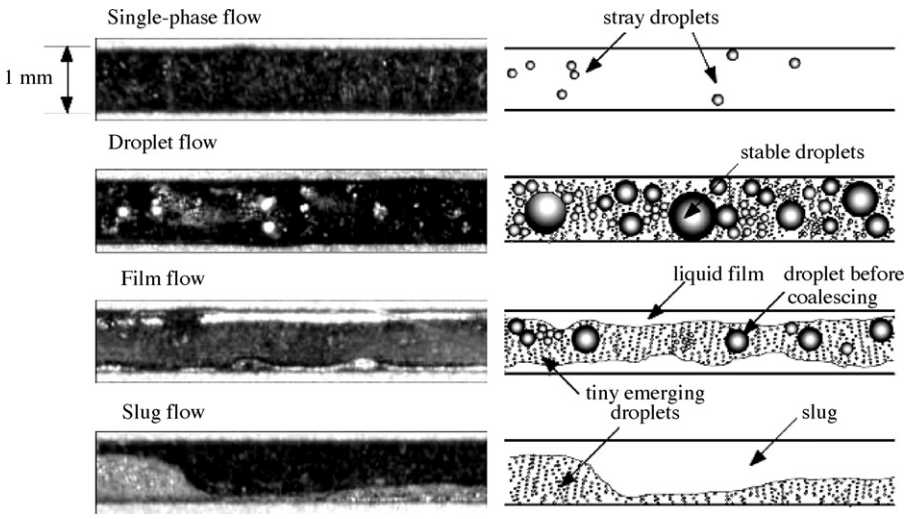

Fig. 4. Typical flow patterns in PEM fuel cell flow channels [30].

a higher degree of channel flooding and thus a higher pressure drop. The pressure drop will continue to increase with time as liquid water accumulates in the channels, which varies with flow rate and flow field design [32]. The flow regime also plays an important role in determining the overall pressure drop, where a liquid slug can completely block a channel before being removed and causing a sudden spike in the pressure drop measurement. Liu et al. [33] have shown that the different flow patterns can be identified based on the total pressure drop. Pressure measurements can also be used to obtain information about how much water will enter the cathode. Differential pressure between the cathode to anode can be used to determine the water saturation in the GDL, which affects how much water is transported into the channel and directly affects the liquid flow rate into the flow channels [34].

The pressure drop can also be used as a diagnostic tool, which is seen by comparing the cathodic pressure drop signal to the voltage signal, as shown in Fig. 6 [2]. As the voltage decreased, the pressure drop increased and fluctuated to a greater extent, providing a sensitive measure of the flooding occurring in the fuel cell. This technique can be useful at the cathode, where major flooding can occur, and at the anode, where little flooding occurs. The anode generally sees little variation in the pressure drop but, like the cathode, the expulsion of slugs coincides with spikes in the pressure signal. Pressure drop measurements on the cathode side have also been used to identify flooding in PEM fuel cell stacks [35,36].

Pressure drop measurements can be used to determine the ideal gas velocity for water removal at a given current density, as shown by Ma et al. [18]. The pressure measurement was compared with photographs in the cell, which showed that as water accumulated, the pressure drop increased. When the water was finally expelled, the pressure drop decreased. As the gas velocity was increased, the magnitude of the fluctuations decreased since droplets did not have adequate time to form in channels and cause a blockage. This type of analysis could help to optimize flow field design and operating conditions, since a reduction in pressure fluctuations can provide more constant output from the fuel cell. One problem associated with pressure drop measurements is that it does not provide information regarding the location of flooding in the fuel cell. However, combining the analysis of the pressure drop measurements with the performance curves can give more insight into the operating regions where flooding is an issue [28].

3.4. Gas reactant flow maldistribution

Typical flow fields for the PEM fuel cell contain multiple channels connected to the same inlet and exit, and non-uniform flow distribution is a major concern. A uniform distribution of current density is considered important in fuel cell operation because it leads to a uniform distribution of temperature and liquid water production, and lower mechanical stresses on the membrane electrode assembly (MEA) [37]. In contrast, flow maldistribution can

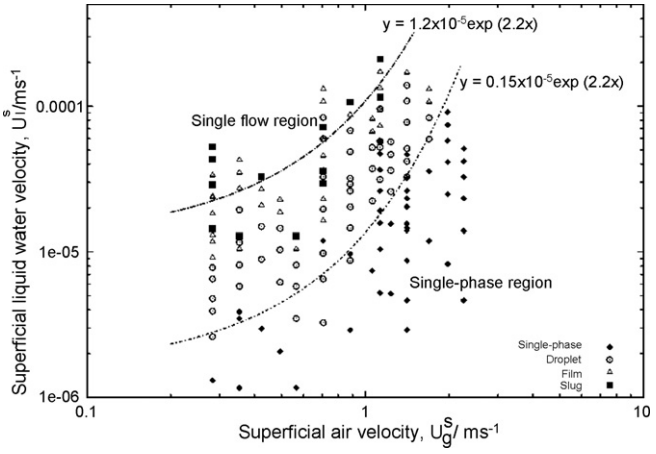

Fig. 5. Flow map in active PEM fuel cells showing different flow regimes [30].

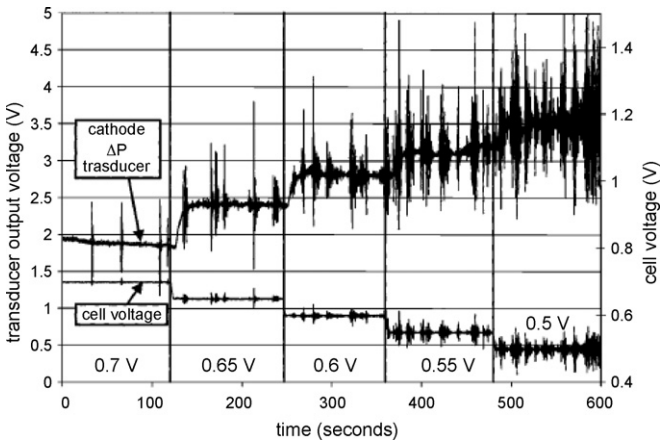

Fig. 6. Pressure drop and voltage signals as flooding diagnostic tools [2].

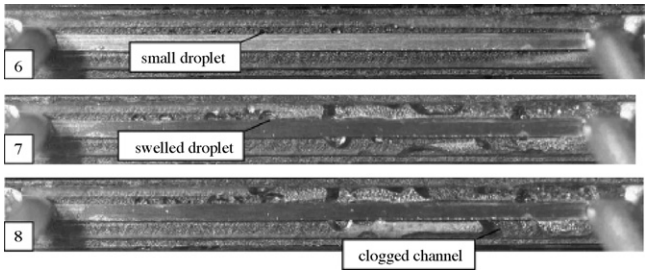

Fig. 7. Flooding in one channel [9].

cause flooding in some channels, leading to a non-uniform distribution of current density and membrane hydration. As a consequence, the pressure drop and current density show erratic fluctuations and the overall power performance decreases. Fig. 7 shows the effects of flooding in a channel [9]. Once the liquid droplet blocks the channel, the cell does not recover itself over the testing period, which impacts the reliability of the PEM fuel cell performance. The occurrence and the recoverability of channel blockage in parallel channels is directly related to the flow instabilities of the two-phase flow in parallel flow channels and is affected by many parameters such as the channel flow rate and the wall physical properties such as the contact angle.

Flow maldistribution in an active fuel cell is considered to be an important factor in reducing the operating lifetime of a fuel cell [38,39]. Therefore, proper gas reactant distribution is critical to ensure high performance and a long lifetime for a PEM fuel cell. Along with visual observation, residence time distributions may help quantify flow maldistribution in PEM fuel cells [40]. Coupling multiple experimental methods will help to further improve our understanding of flow maldistribution in fuel cells.

4. Ex situ experimental two-phase flow studies relevant to PEM fuel cells

Since two-phase flow is a complex phenomenon in PEM fuel cells, ex situ studies enable one to explore detailed mechanisms behind intricate two-phase flow behavior at flow conditions relevant to fuel cell operations. In some cases, the work is tied directly to PEM fuel cells, such as droplet emergence and detachment in channels from a GDL surface. Other cases involve non-fuel cell applications, such as heat exchangers, where two-phase flow is also relevant. Ex situ experiments possess the advantages of easy equipment setups, flexible operating conditions, and the ability to decouple reaction and heat and mass transfer from intricate flow phenomena. This section presents an overview of existing ex situ experimental results related to two-phase flow in minichannels with relevance to fuel cells. These studies have explored the influence of flow conditions, channel wall wettability, channel geometries, and flow media on hydrodynamic parameters such as droplet formation, pressure drop, flow pattern, and liquid holdup. In the other cases, flow distributions are investigated in parallel channels, though few studies are concerned with this phenomenon [41,42].

As noted in Section 3, gas–liquid two-phase flow in PEM fuel cells is unique to other applications. Significant differences from conventional two-phase flow can arise from large gas to liquid flow ratios, the method of liquid introduction, and a combination of several water transport mechanisms including electroosmotic drag, back diffusion, and water condensation from humidified inlet gases. To simulate an operating fuel cell, the water production rates and total water transport can be taken into account using Faraday's law modified with a water transport coefficient, α, for water transport across the MEA as follows:

$$m_{\text{water}} = \frac{(1+2\alpha)iA_{\text{act}}}{2F} \tag{5}$$

where m_{water} is the rate of moles of water generated on the cathode side, A_{act} is the active area (cm^2), i is the current density (A cm^{-2}), and F is Faraday's constant ($96{,}485\,\text{C mol}^{-1}$). Air instead of pure oxygen is commonly used as the oxidant gas at the cathode side and the corresponding superficial gas velocity can be calculated by

$$u_G = \frac{2.38\lambda M_{\text{air}}}{\rho_{\text{air}} A_{\text{channel}}} \frac{iA_{\text{act}}}{4F} \tag{6}$$

where A_{channel} is the cross-section area of the flow channels, m^2. The corresponding superficial velocity of air ranges from 0 to $10\,\text{m s}^{-1}$, analogous to active fuel cell operations in the current density range of 0–$2\,\text{A cm}^{-2}$ and gas stoichiometric ratios up to 20. Experimental conditions in all two-phase flow studies for fuel cell applications generally fall into those flow conditions, with gas flow channel dimensions typically in the sub-millimeter to millimeter range.

Table 2 summarizes ex situ experimental studies of two-phase flow related to fuel cell operation in the literature.

4.1. Flow patterns

In the ex situ experiments, flow patterns were investigated under flow conditions related to fuel cell operation. Flow patterns are dependent on the superficial gas and liquid velocities, which can then be related to gas flow stoichiometric ratios and current densities under active fuel cell operation. In the literature, there are various flow regimes observed in different experiments depending on the flow operating conditions, channel geometries, and liquid water introduction methods. Flow hysteresis is also observed in minichannels bounded with porous walls [45]. Additionally, channel wettability largely influences the flow regimes in gas flow channels [43].

Similar to the flow regimes identified in the in situ experiments, typical flow regimes of ex situ two-phase flow relevant to fuel cells are shown schematically in Fig. 8.

The gray in the figure represents liquid water while the clear areas represent air. Various researchers have observed the flow regimes shown in Fig. 8. These include slug flow (Fig. 8(a)) where a discrete droplet grows to or close to the size of the channel, blocking gas passage [6,43], transition flow from slug flow to annular flow (Fig. 8(b)) [6], wavy-stratified flow (Fig. 8(c)) [26], and stratified (or annular) flow (Fig. 8(d)) that occurs at high superficial gas velocities with low pressure drop fluctuations [6]. Lu et al. [47] found that at low gas velocities (typically stoichiometric ratios below 5) slugs or semi-slugs are in dominance, leading to severe flow maldistribution in parallel channels and large fluctuations in pressure drop. They have also reported a mist flow, which is considered an effective way to remove water because liquid droplets are dispersed in the gas phase and removed convectively. However, mist flow requires high gas velocities, resulting in high parasitic power losses

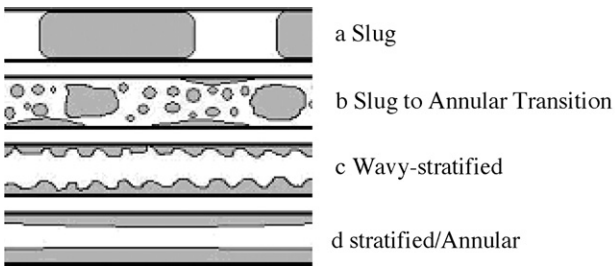

Fig. 8. Flow patterns in PEM fuel cell operations (a) slug flow, (b) transition flow from slug to annular, (c) wavy-stratified, and (d) stratified (annular) flow.

Table 2
Ex situ experimental studies of two-phase flow in minichannels and microchannels for fuel cells.

Authors	Channel dimensions	Operation conditions	Remarks
Allen [43]	330 μm circular and 500 μm square	Nitrogen and water, u_G = 0–2.4 m s^{-1} and u_L = 0–0.035 m s^{-1}	Non-wetting channels with high flow resistance
English and Kandlikar [44]	1.124 mm in width and 0.93 mm in height	Air, water and surfactant Triton DF-12 with concentrations of 0.0208–0.1089; u_G, 3.19–10.06 m s^{-1} and u_L, 0.0005–0.022 m s^{-1}	No significant difference in pressure drop in different surfactant solutions
Lee et al. [45]	0.5 mm in width and 0.2 mm in depth	Air and water; u_G, 0–20 m s^{-1}; u_L, 0–0.007 m s^{-1}	Flow hysteresis; flow regimes depends on GDL hydrophobicity
Zhang et al. [41,46]	Y-branched parallel channel, 1.6 mm in width and 1.6 mm in height	Air and water; u_G: 0–10 m s^{-1}; u_L: 0–0.03 m s^{-1}	Flow hysteresis, flow maldistribution occurs at low gas and liquid flow rates
Lu et al. [47]	Parallel channels, 0.7 mm in width and 0.4 mm in height	Air and water; u_G: 0–20 m s^{-1}; u_L: 0–0.015 m s^{-1}	Two-phase flow patterns, pressure drop in parallel channels, flow maldistribution
Kandlikar et al. [42]	Parallel channels, 0.7 mm in width and 0.4 mm in height	Air and water; u_G: 0–20 m s^{-1}; u_L: 0–0.0003 m s^{-1}	Entrance region pressure drop measurement; flow maldistribution due to different flow resistances

when applied to an operational fuel cell. Film flow or stratified flow is therefore considered to be the most favorable flow pattern for water removal from the gas flow channels because it requires a minimum gas velocity to achieve the desired flow pattern. As previously discussed, Trabold [2] found that a superficial gas velocity of 5–6 m s^{-1} is needed to achieve this flow pattern while Lu et al. [47] found the superficial gas velocity should be more than 3 m s^{-1}. These results are shown in Fig. 9, with the main regimes being slug, film and mist flows.

Flow pattern maps have been generated in terms of superficial gas velocities and superficial liquid velocities for other applications as well. Examples of flow pattern maps for conventional air and water studies can be found in Refs. [48–51]. While not directly related to the conditions experienced in a PEM fuel cell, these works provide a strong framework from which PEM fuel cell two-phase flow studies can emerge. The bubbly flow pattern is not observed in PEM fuel cells due to the required high ratios of liquid flow rates to gas flow rates. In microchannels, the surface tension, inertia, and viscosity are important parameters. These forces can be combined to form several dimensionless groups as discussed by Akbar et al. [49], which may help create dimensionless flow regime maps with greater relevance to fuel cells.

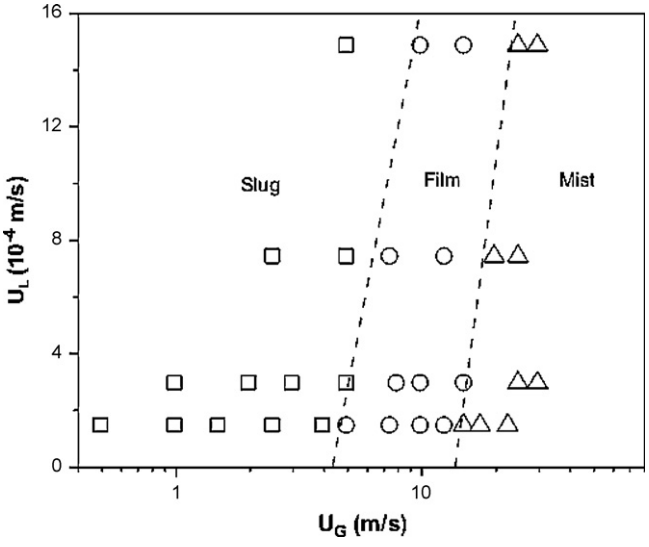

Fig. 9. Ex situ flow patterns in terms of superficial gas and liquid velocities [47].

4.2. Gas reactant flow maldistribution and hysteresis

Uniform distribution of gas reactants in fuel cell flow fields is important for fuel cell performance. Non-uniform flow distribution can lead to performance losses and non-uniform gradients. In the literature, few attempts have been made to simulate fuel cell flow fields to address this critical issue due to the complexity of the flow distribution in active fuel cell flow fields. This complexity arises from a number of factors including the presence of the porous gas diffusion layer, where pressure gradients can cause leakage of reactant gas between flow channels. Therefore, gas flow rates (and local stoichiometry) can differ from one end of the gas flow channels to the other and differ between channels. Traditional two-phase flow studies in other applications (such as heat exchangers) on maldistribution can be found in Refs. [52–54]. These studies are useful references for furthering two-phase flow studies related to PEM fuel cells.

The gas flow rate in the entrance region of individual channels can be used as an indicator of flow distribution in the flow fields, since no other measure is available to characterize this effect to the best of our knowledge. Kandlikar et al. [42] developed an entrance region pressure drop measurement technique to determine instantaneous gas flow rates through individual channels. The method was employed in both an ex situ and in situ experimental setup, and it was found that a porous GDL backing could lead to severe flow maldistribution compared to impermeable backing for the same channels. At in situ operating conditions, flow maldistribution was also observed due to water blockage in gas flow channels. One limitation of this method is difficult implementation in operating fuel cells. Nevertheless, it still can provide valuable information of flow maldistribution in parallel channels related to other fuel cell operating parameters such as current density, gas stoichiometry, and gas humidity in a fuel cell with specially designed introduction.

The order of changing gas flow rates on flow distributions also has an impact on flow distributions in parallel channels. In recent work by Zhang et al. [41,46] on gas–liquid flow patterns and flow distributions in two parallel channels, it was found that flow maldistribution occurred at low gas and liquid flow rates, corresponding to low gas stoichiometric ratios, where slug flow patterns were observed. In addition, flow hysteresis phenomena were also found when the gas flow rate was changed in an ascending or a descending manner. Fig. 10 shows an experimental flow regime map representing the flow patterns in two parallel channels for superficial gas velocities changed in an ascending and descending manner.

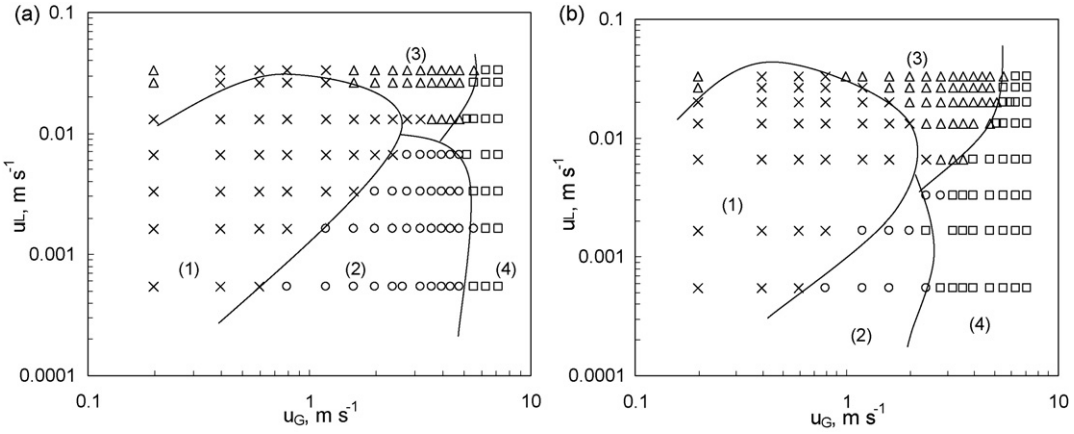

Fig. 10. Flow patterns in parallel channels as observed at different superficial gas velocities and liquid velocities (a) ascending approach and (b) descending approach. (1) ×: slug flow + stagnant liquid; (2) ○: stratified flow + stagnant liquid; (3) Δ: slug flow in both channels; (4) □: stratified flow in both channels; solid lines are drawn as guides to the eye and define boundaries between flow patterns. [46].

When the system starts from initial flooding conditions, stratified flow in both channels (regime 4) cannot be reached until very high gas velocities. Slug flow in both channels (regime 3) occurs at medium levels of gas flow rates and high liquid flow rates. Both regime 4 and regime 3 indicate even flow distributions. However, at low gas velocities the gas tends to go through one channel preferentially, leaving the other channel filled with liquid only, as shown in regime 1 and regime 2. This observation is consistent with previous work [55,56] that at low gas velocities both gas and liquid tend to flow in one channel of parallel channel systems, leading to a flow maldistribution. Fig. 10(b) shows the flow pattern distribution identified with decreasing the gas velocity from a stratified flow condition. Compared to the flow patterns obtained in the gas ascending process (Fig. 10(a)), there is a wider region for slug flow and stratified flow in both channels (regime 3 and regime 4) in the gas descending process. In addition, the region of stratified flow and stagnant liquid (regime 2) appears to be much narrower in the gas flow descending process. Flow hysteresis and flow maldistribution are also observed from the pressure drop data shown in Fig. 11.

It is seen in Fig. 11 that with an increase in inclined angles the total pressure drop increases due to the additional gravitational or static pressure drop. In general, there is a slight decrease in the pressure drop with an increase in the superficial gas velocities, followed by an increase in the pressure drop with further increasing superficial gas velocities. However, the occurrence of the sudden change in pressure drop indicates a transition from flow maldistribution to even distribution. It was also found that the pressure drop at the peak reflects intrinsic characteristics of the channel design and a lower value is always desirable, indicating that a lower gas flow rate is required to purge water slugs in the gas flow channels. In addition, the hysteresis zone still exists in parallel channels inclined with a positive angle, whereas flow hysteresis disappears at negative angles with even flow distribution achieved at lower gas velocities. This result indicates that it might be beneficial to position flow fields downwards during real fuel cell operation.

While it has been recognized that the presence of liquid slugs in the gas flow channels leads to flow maldistribution [28,42], theories or models to interpret instability-induced flow maldistribution are still lacking in the open literature. An attempt was made recently to analyze the stability of possible solutions of gas and liquid flow distributions in parallel channels for fuel cells with a one-dimensional momentum balance equation across the channels [41]. All possible combinations of gas and liquid flow distributions must satisfy the equal pressure drop across all channels if they share a common inlet and outlet. Theoretically, even flow distribution is one default solution of the equal pressure drop requirement, but experimental results show that an even distribution is not always observed. Instead, flow maldistribution appears as a stable solution, indicating that flow distributions of two-phase flow in parallel channels depend on not only pressure drop but also flow stability. If the

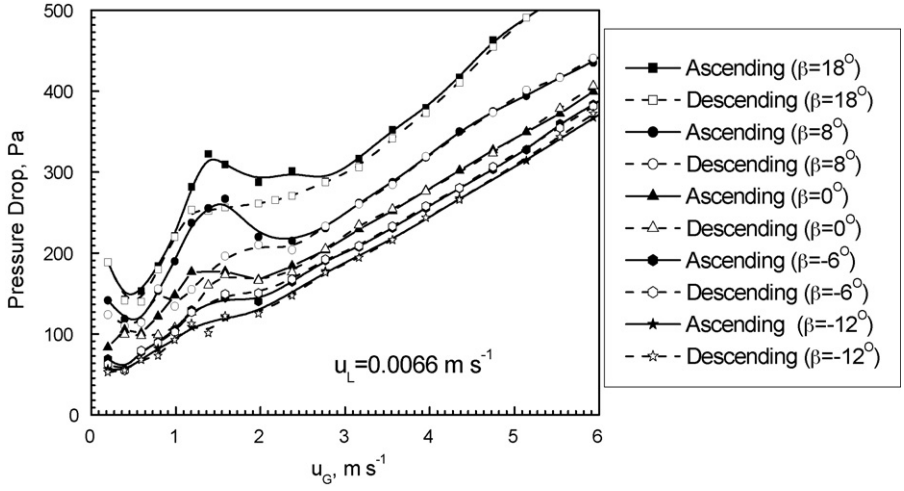

Fig. 11. Effects of inclination angles on pressure drop in two different approaches [41].

two-phase flow is operated at an unstable condition, a small perturbation will shift the flow to the nearest stable conditions. A more rigorous theoretical analysis should be conducted over a wide range of operating conditions in the future.

4.3. Droplet generation and removal

In the fuel cell, water can enter the gas flow channels from the gas diffusion layer (GDL) media and the behavior of these droplets is important in understanding the development of two-phase flow. Schillberg and Kandlikar [57] provided a detailed review of water droplet detachment mechanisms, summarizing relevant operating variables such as the channel dimensions, droplet sizes, Reynolds number, GDL properties, temperature, water introduction rate, and gas flow conditions. Their review also covered the approaches taken to study the type of flow, drag forces, and surface adhesion forces reported in the literature. A static force balance on a droplet emerging from a GDL into a flow field is given by

$$F_P + F_{shear} + F_{drag} = 0 \quad (7)$$

where F_P is the pressure force from the flow field pressure gradient, F_{shear} is the shear force exerted on the top wall by the fluid, and F_{drag} is the drag force exerted on the droplet by the bottom GDL, which is equal and opposite to the surface tension/adhesion force before the droplet detaches from the GDL [58]. If the drag force balances the adhesion force, the droplet will not be removed and the droplet is considered stable. Increasing the drag force until it is greater than the adhesion force can cause instability, allowing the droplet to be detached from the GDL. Kumbur et al. [58] further developed equations for these forces and provided a final macroscopic force balance containing relevant parameters such as the contact angle hysteresis (difference in advancing and receding contact angles), flow velocity, droplet height, chord length, and the channel height. The results of their analysis are in good agreement with experimental results. An important conclusion of this study is that for a constant droplet size and channel width, a lower channel height aids in droplet removal.

When water permeates through the porous GDL, the droplet grows until the force of gravity or the shearing of the liquid by the gas overcomes the surface adhesion force between the droplet and the pore [57]. The liquid water droplets appear in preferential areas, rather than uniformly along the channel [48,53,59]. Once detached, the droplet moves along the GDL surface, where it can combine with other droplets to form slugs [60]. The droplet formation from the GDL surface in PEM fuel cells is difficult to study and simulate in ex situ experiments. Water is often introduced between the middle and the end of the channels instead of uniformly along the channel. Also, droplets have been identified in two categories: land-touching and non-land-touching, and those that touch the lands grow faster and to a larger size [7]. The location where water droplets are first observed also changes over long operating time (3000 h). Observed at 161, 2036, and 3092 h, the emergence of droplets moved towards the exit with time [61]. However, most ex situ two-phase flow studies are carried out over short time periods (typically <1 h at each data point), and conclusions drawn from these ex situ studies on droplet dynamics may not be accurately capturing fuel cells with long expected lifetimes, such as 5000 h for cars, due to cell degradation [62].

Addition of water to the anode channel can also affect cell performance. After a long time (>1 h) and at low current densities ($i < 0.2\ A\ cm^{-2}$) water can move into the anode due to a concentration gradient across the membrane. Characterizing two-phase flow in the anode channel may also be important when a micro-porous layer (MPL) is used. The MPL on the cathode creates a pressure barrier, which forces water to the anode side rather than to the cathode side [12].

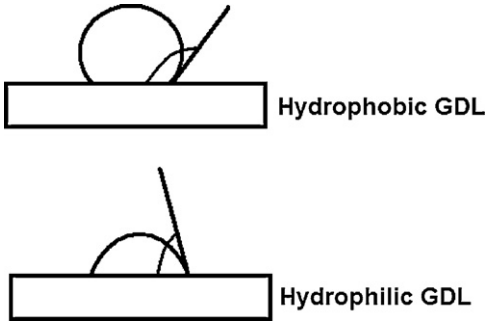

Fig. 12. Effect of hydrophobicity on contact angle.

From experiments [63], it has been established that the droplet formation and critical detachment diameter on the cathode side GDL are a function of the air flow rate, water injection rate, and material contact angles. For instance, a standard Toray carbon fiber paper (without PTFE treatment) is highly wettable, which facilitates water spreading instead of forming droplets. The droplet dynamics under hydrophilic and hydrophobic conditions are schematically illustrated in Fig. 12.

When the contact angle is less than 90°, the surface is hydrophilic and the droplet wets the surface; when the contact angle is greater than 90°, the surface is hydrophobic and the droplet beads up on the surface. The hydrophobic cases allow a droplet to reach a critical diameter (depending on the gas and liquid flow rates) and then detach. However, when the surface is hydrophilic, the droplet does not detach and remains on the surface, blocking oxygen diffusion into the GDL and starving the electrochemical reaction. The contact angle of the channel wall is also an important parameter. Theoretically, water film formation along the channel is dictated by the Concus-Finn condition [64]:

$$\theta + \alpha < \frac{\pi}{2} \quad (8)$$

where θ is the contact angle of water on the channel and α is the half-angle formed by the channel corner. For a rectangular channel, α is equal to 45°. The wall contact angle has to be lower than 45° in order to achieve film formation along the flow channels. In PEM fuel cells, the channel walls are usually hydrophilic, and more hydrophilic channel surfaces are desired for proper water management since film flow is considered to be a preferable flow pattern for water removal in fuel cells.

Ous and Arcoumanis [7] showed that the air velocity that caused detachment is inversely proportional to the droplet size, i.e., smaller droplets detached at higher velocities. Taller droplets are easier to remove than flatter droplets due to a greater drag force relative to the surface adhesion force. Polytetrafluoroethylene (PTFE) loading causes the droplet to bead up, which can increase contact angle hysteresis and therefore more deformation occurs. Greater deformation of the droplet decreases the surface tension between the water and carbon fiber paper, leading to detachment. Temperature is also an important variable in the droplet detachment process. As the temperature increases, the surface tension decreases, which allows droplets to be removed from the GDL at lower velocities [14]. Recently, an innovative approach used fluorescence microscopy to monitor droplet movement, where a stagnant drop on a hydrophobic GDL moved quasi-statically across the GDL with a dynamic solid surface to mimic the landing area [65]. The hydrophobic landings remove water more effectively under the landing areas, facilitating quick water detachment into the flow channel.

The effect of advancing and receding contact angles is also important. The definitions of hydrophilic and hydrophobic surfaces given above are in reference to a static droplet. However, when the

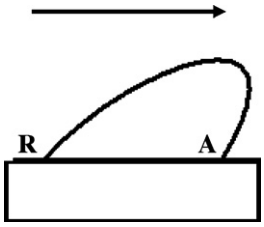

Fig. 13. Contact angle hysteresis showing direction of flow and the resulting advancing and receding contact angles.

air flows over the droplet, the droplet deforms and two contact angles are created. These are referred to as advancing and receding contact angles and are also called contact angle hysteresis, which must be considered when modeling droplet detachment from a GDL surface [9]. A schematic of the dynamic behavior of a droplet with contact angle hysteresis is shown in Fig. 13.

Fang et al. [66] further showed the importance of contact angle hysteresis in a numerical simulation, where the contact angle hysteresis is found to impact slug elongation and detachment. The model agreed well with the deformation of droplets measured in microchannels.

The capillary number, which ratios the viscous force exerted on a drop by the air to the surface tension, has been used to characterize the deformation of a droplet. The capillary number, *Ca*, is defined as

$$Ca = \frac{\mu V}{\gamma} \tag{9}$$

where μ is the viscosity and V is the velocity of the continuous phase (in this case air) and γ is the interfacial surface tension. Over the range of *Ca* from 0.014 to 0.219, droplet deformation was studied numerically on a solid surface and it was found that the deformation was a strong function of *Ca* when it is large [67]. Droplet detachment can also be characterized by a critical *Ca*, which corresponds to the point that the advancing and receding contact angles reach an observable limit [14]. These results were studied numerically and experimentally on GDL surfaces relevant to fuel cells.

Different fabrication techniques can alter the surface roughness, which is often only reported from the manufacturer as an average value [68]. The surface roughness is especially important for channels with small hydraulic diameters (0.62–1.067 mm), as the pressure drop and heat transfer can be increased with increased surface roughness [69]. The work of Dunbar and Masel [26] suggested that the slugs of liquid water in the channels (monitored by MRI) often move from surface defect to surface defect. These findings suggest that the surface roughness plays a role in two-phase flow in PEM fuel cells.

5. CFD simulations of two-phase flow in PEM fuel cell flow channels

In recent years, several reviews have been published about the fuel cell models. Weber and Newman [70] presented various types of transport and corresponding models in each fuel cell layer. However, their review mainly focused on one-dimensional models and two-phase flow in gas channels was not taken into account. Wang [71] summarized fundamental models for PEM fuel cell engineering but limited the review to computational fluid dynamic (CFD) methods only. Biyikoglu [72] presented a review about different aspects of modeling and simulation, including CFD modeling and flow field design. Tao et al. [73] presented a comprehensive review of mathematical modeling of PEM fuel cells, which especially focused on model validation and parameter influence. Djilali and Sui [74] gave a critical discussion about computational strategies for the polymer electrolyte membrane, porous gas diffusion electrodes, and microchannels. Multi-scale strategies were also discussed. Most recently, Siegel [75] presented a detailed literature overview of PEM fuel cells models with a focus on modeling strategies and commonly used model assumptions. However, no review has been written to the authors' knowledge focusing on the presence of two-phase flow in the gas channels of PEM fuel cells.

5.1. Gas–liquid two-phase flow models for PEM fuel cells

Empirical models, mechanistic models, and computational fluid dynamics (CFD) models have been developed to study the gas–liquid two-phase flow. In PEM fuel cells, gas–liquid two-phase flow occurs simultaneously with mass transfer, heat transfer, and electrochemical reactions, and is affected by the material properties in different components. Therefore, CFD models can be effective tools for the numerical investigation of two-phase flow phenomena in PEM fuel cells. Liquid water transport was first incorporated in fuel cell modeling in early 2000, with these works treating the liquid water as a solid species that only occupies a certain volume fraction [76] or neglecting the convective transport of liquid water [77]. As computational power increased, more complex two-phase flow models have been applied to the PEM fuel cell modeling. In this section, several two-phase flow models applied to PEM fuel cells are reviewed, including the multi-fluid model, mixture model, volume of fraction method (VOF), and Lattice Boltzmann method (LBM). Table 3 summarizes the current literature on CFD simulations of gas–liquid two-phase flow in PEM fuel cells.

The multi-fluid model was first used in PEM fuel cell modeling by Berning and Djilali [78]. In this model, each phase is represented by one complete set of conservation equations (mass, momentum, and energy), and the two phases are coupled by the saturation state. This model has only a few assumptions, but requires the highest number of dependent variables, and the coupling of the phases can lead to unstable solutions [79].

The mixture model was first used to model PEM fuel cells by Wang et al. [80] and uses the same equation set as the multi-fluid model. Each phase is modeled using an individual mass conservation equation, but a single momentum equation is solved to obtain the velocity field of the mixture, of which physical properties are the average of the two phases. Each phase velocity can then be extracted from the mixture velocity in the post-processing. Recently, Gurau et al. [81] commented that the mixture model was limited to flows without phase transitions or phase production because the momentum term due to phase change is neglected. For more complex situations, such as in PEM fuel cells, this model may lead to predictions of unrealistic velocity and scalar fields. Although Wang's group [82] responded that the "missing" term was relatively small compared with the Darcy term, Gurau [83] insisted that the missing term possibly had the same order of magnitude as the Darcy term.

The volume of fraction (VOF) method was developed in the 1970s as a flexible way to simulate complicated free boundaries [84] and this method has become popular in simulating gas–liquid flows in fuel cell gas flow channels since first applied by Quan et al. [85]. The model can simulate immiscible fluids by solving a single set of momentum equations and then tracks the volume fraction of each of the fluids throughout the domain. Due to its capacity to consider surface tension and wall adhesion effects, liquid droplet behaviors can be captured and traced. Thus, this model is especially suited for surface tension dominated flows and flows in channels with different wall materials. However, because the specific structure of the flow domain is required this model has been only applied to gas flow channel simulations, and it is difficult to couple to the electrochemical reactions in the fuel cell.

Table 3
Selected studies on modeling of gas–liquid two-phase flow on PEM fuel cells.

Models	Authors	Research aspects	Remarks
Mechanistic model	Chen et al. [87]	Effects of gas flow velocity, flow channel length and height, and contact angle hysteresis on the droplet detachment diameter	No water injected, single sphere droplet
	Chen [88]	Effects of channel height, contact angle hysteresis and water-droplet size on the critical gas flow velocity	No water injected, single sphere droplet
Multi-fluid model	He et al. [89]	Effects of wettability on the droplet detachment diameter	Single droplet
VOF	Theodorakakos et al. [14]	Effects of temperature on the droplet detachment	Single water inject pipe
	Zhan et al. [90]	Effects of gas flow velocity, wettability and flow channels on the droplet removal	Liquid water was injected from the same inlet as gas
	Cai et al. [91]	Effects of wettability on the droplet removal.	Liquid droplet was initially attached to the GDL surface
	Shirani and Masoomi [67]	Effects of gas velocity, the density and viscosity of water, and the surface tension coefficient on the flow pattern	No water injected, single droplet
	Zhu et al. [92]	Effects of channel size and pore diameter on the water droplet motion	Single pore, high liquid flow rates
	Bazylak et al. [93]	Effects of GDL microstructure on the droplets motion	Only two water inject pipes
	Zhu et al. [94]	Effects of wettability of channel walls, pore diameter, gas velocity, and liquid water velocity	Single pore, high liquid flow rates
	Zhu et al. [95]	Effects of air and water velocity, pore diameter and the wettability of the GDL surface	Single pore, high liquid flow rates
	Fang et al. [66]	Effects of contact angle hysteresis	Single water inject pipe
	Le and Zhou [96]	A 3D general model of PEM fuel cell coupled VOF method	Homogenous GDL and electrode
	Le and Zhou [97]	Flow behaviors of liquid water in serpentine-parallel flow channels	Homogenous GDL and electrode
	Quan et al. [85]	Behavior of liquid water in a U-shaped serpentine gas channel	Liquid water was initially attached to the GDL surface
	Jiao et al. [98]	Behavior of liquid water in a complex parallel serpentine channel	Liquid water was initially attached to the GDL surface
	Jiao et al. [99]	Air-water flow in a 3D straight micro-parallel-channel	Liquid water was initially attached to the GDL surface
	Quan and Lai [100]	Effects of channel wettability, channel geometry, and air inlet velocity on water behavior	Homogenous GDL
	Jiao and Zhou [101]	Investigation on three innovative GDLs microstructure designs	Homogenous catalyst layer
	Jiao and Zhou [102]	Effects of electrode wettability	Homogenous catalyst layer
	Ding et al. [110]	Two-phase flow pattern, effects of GDL microstructure, surface wettability, liquid flow rates	Multiple pores, simplified GDL surface
LBM	Hao and Cheng [103]	Effects of gas velocity and GDL wettability	Single pore
Mixture model	Wang et al. [104]	Effects of air stoichiometry and relative humidity	Homogenous electrode and GDL
	Basu et al. [105]	Effect of GDL intrusion at the edge channels	Homogenous electrode and GDL
	Basu et al. [106]	Maldistribution effects in parallel channels	Steady-state and isothermal

Instead of solving the Navier–Stokes equations like traditional CFD methods, the Lattice Boltzmann method models the fluid as fictive particles, which perform consecutive propagation and collision processes over a discrete lattice mesh. In conventional CFD models, it is difficult to implement microscopic interactions, such as interfaces between gas and liquid phases, into the macroscopic Navier–Stokes equation. However, in the LBM, the particulate kinetics provides a relatively easy and consistent way to consider the microscopic interactions by modifying the collision operator [86]. Thus, this method shows great potential to simulate the two-phase flows in PEM fuel cells. Unfortunately, as a mesoscopic model, it is difficult to apply this method to large length scales, and coupling this model with heat transfer and reactions is still a challenge.

5.2. CFD simulations of two-phase flow in gas flow channels

5.2.1. Droplet behavior

Understanding the liquid water motion in gas flow channels is essential for effective water management in a PEM fuel cell. Early two-phase flow models always assumed the liquid water moving at the same velocity as the gas flow, called mist flow [107,108]. However, as discussed in Section 3.2, in situ experiment results showed that water emerging from the GDL surface formed droplets rather than mists (Fig. 14), especially at a high current density or a low gas stoichiometric ratio. Therefore, the droplet behavior in the gas flow channel must be well understood to accurately characterize two-phase flow in the gas channels.

The critical detachment diameter of a droplet is different with respect to changing operating conditions, channel design, or using different materials. Chen et al. [87] developed a two-dimensional simplified cylindrical droplet model to predict the instability of a single water droplet based on macroscopic force balances and a droplet-geometry approximation. Their qualitative results indicated that increasing the flow channel length or mean gas flow velocity, decreasing channel height or contact angle hysteresis, or making the GDL surface more hydrophobic would reduce the critical detachment diameter and enhance the removal of droplets. The same model also predicted the critical gas velocity required for a spherical water droplet to detach from the GDL surface [88]. It was found that the critical gas velocity varied inversely with water-droplet size (to the 2/3 power), and decreased with increasing GDL surface hydrophobicity, decreasing contact angle hysteresis, and lowering the channel height. However, the geometry approximation used in this simplified model would result in an inaccurate drag force on the droplet, especially at high gas flow velocity. Parametric studies with the VOF method [92] showed that the height of the channel as well as the width of the pore had a significant impact on the detachment of the water droplet. The critical velocity was found to decrease with increasing droplet size and decreasing GDL pore diameter. Zhu et al. [109] also investigated the effects of channel geometry on the droplet dynamics. Lower aspect ratios reduce the GDL coverage ratio due to droplets attaching to the top wall, but lower aspect ratios also increase the pressure drop. A rectangular channel with a curved bottom wall was found to have

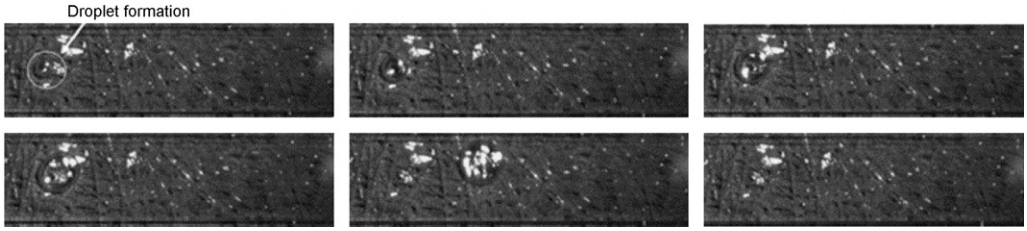

Fig. 14. Visualized water droplet formation and detachment from the GDL surface [14].

a minimum coverage ratio and water saturation and a moderate pressure drop. However, the liquid flow rates in their simulations were much higher (several orders) than those in a realistic PEM fuel cell and the droplet motion may be quite different at low liquid flow rates corresponding to real fuel cell operation.

More hydrophobic GDL surfaces aid in droplet detachment because of lower capillary forces, as shown by He et al. [89] using the multi-fluid model. These results are in agreement with Hao and Cheng [103], who applied a multiphase LBM approach to show that high gas flow velocities and a more hydrophobic GDL surface were beneficial for the water removal. An analytical model based on a force balance was also developed to predict the droplet detachment size. Zhu et al. [94] found that the critical air velocity for detachment decreased with increasing hydrophobicity of the surface and increasing the initial size of the droplets. Temperature also has an effect on the droplet's detachment [14]. Experimentally measured contact angles and operating conditions were input into a numerical model based on the VOF method where water was injected from a single pipe. The results showed that higher temperatures facilitate the droplet's detachment due to lower surface tension and adhesion forces. Contact angle hysteresis plays a major role in droplet detachment dynamics. Fang et al. [66] investigated the effects of contact angle hysteresis on the droplet detachment height using the VOF method and showed that without considering the contact angle hysteresis, the droplet's detachment height was quite different from what was observed in the experiments. These results are shown in Fig. 15. The results also implied that the contact angle distribution along the droplet can be approximated by piecewise linear functions.

After detachment, a liquid droplet may have different behavior while moving along the gas flow channel because of different operating conditions or materials (different wettabilities of channel surfaces). A hydrophobic GDL surface and hydrophilic channel sidewall, which is a common condition in PEM fuel cells, turns dispersed droplets into thin water films attached to the channel sidewalls [91]. Shirani and Masoomi [67] also used the VOF method to investigate the motion of a liquid droplet. By studying the effects of gas velocity, the density and viscosity of water, and the surface tension on the droplet deformation, it was found that the droplet shape strongly depended on the capillary number when the capillary number was large and poorly correlated with the Reynolds number.

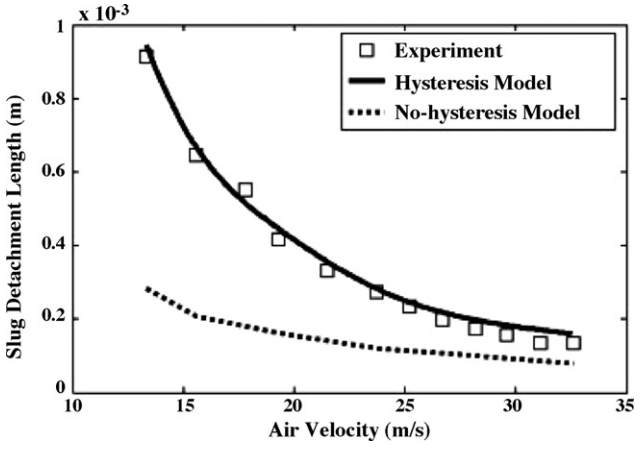

Fig. 15. Droplet detachment height versus air velocity. Both hysteresis and non-hysteresis results are presented for comparison with experimental results [66].

5.2.2. Flow patterns in a PEM fuel cell

In the above section, the focus was mainly on the dynamics of a single droplet. However, in PEM fuel cell gas channels, droplets always emerge from GDL surface at multiple sites. Thus, the two-phase flow pattern can be different from the single droplet behaviors discussed above due to the coalescence of droplets.

Bazylak et al. [93] studied multi-droplet effects by employing two pipes to represent the microstructure of the GDL. With an initially dry GDL and gas channel, slug flow and channel flooding followed the motion of individual droplets. More recently, Ding et al. [110] studied the effect of the GDL surface microstructure by varying the pore diameters and the number of pores with the VOF method. Three stages were identified during the droplet formation: droplets merging on the GDL surface, accumulation on the channel sidewalls, and detachment from the top wall. These results are shown in Fig. 16. The results also showed that different GDL surfaces would result in significantly different two-phase flow patterns. However, when the pore size was small enough (and the pore number was large enough), the flow pattern would not change with further reduction in the pore diameter. This result suggested that the GDL surface microstructure could be simplified by increasing the pore size to reduce the computational time. The material wettability had a strong impact on the two-phase flow pattern and pressure drop, where more hydrophilic sidewalls or more hydrophobic GDL surfaces were beneficial for water removal.

Jiao and Zhou [101] used several small cubes or trapezoids with the same volume to represent the pores from which liquid water could emerge from a GDL. The results indicated that the trapezoidal porous holes with the minimum area facing the gas flow channel were beneficial to the liquid removal due to enhanced air flow inside the GDL. Furthermore for these microstructure designs, the hydrophobicity level of the catalyst layer must be greater than or equal to the GDL in order expel liquid water into the gas flow channel [102].

Channel design is another key factor that affects the two-phase flow pattern. In fact, the appropriate design of flow channels has been considered the most successful strategy in addressing water flooding issues [1]. Three commonly used flow fields in PEM fuel cells are parallel/straight channels, serpentine channels, and interdigitated channels.

Zhan et al. [90] showed that straight channels with high air velocities and more hydrophobic surfaces are beneficial to the liquid water removal. However, in this study liquid water was injected with the inlet gas, which is different from droplets emerging from GDL surfaces in real PEM fuel cells. Simulation results using the VOF method indicated that the bend area inside a U-shaped microchan-

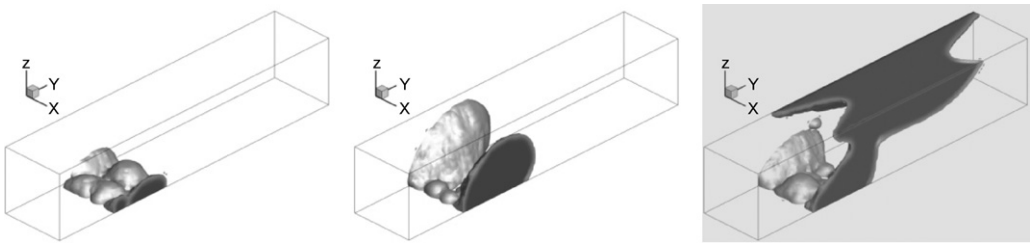

Fig. 16. Three stages of the emerging water droplet into a channel: (a) merging, (b) accumulating, and (c) detaching [110].

nel played an important role in determining water behavior [85]. Water flooding could occur in the "after-bend" section, and, with larger amounts of water, the water distribution following the U-bend can block the reactant transport inside the flow channel. However, liquid droplets were initially placed in the channel, which is different from an actual PEM fuel cell where the droplets emerge from GDL surfaces. Jiao et al. [98] presented a numerical investigation of two-phase flow in a more complex parallel serpentine channel format with manifolds with water droplets initially placed in the channel. Using the VOF model, the serpentine gas flow channel's "collecting-and-separating-effect" facilitated water drainage, and it was recommended that keeping the area that has the higher amount of water close to the outlet manifold was beneficial for water drainage. Jiao et al. [99] further simulated a 3D straight micro-parallel-channel format with PEM fuel cell stack inlet and outlet manifolds. It was found that the outflow manifold might be easily blocked by water even if the amount of water was small. A curved channel wall was suggested to prevent water from flowing back to the air inlet, allowing water to move into the flow field channels faster.

Quan and Lai [100] numerically investigated the effects of channel surface wettability, channel geometry, and air inlet velocity on water behavior, water content inside the channel, and two-phase pressure drop. The results showed that the pressure drop was caused by channel blockage and the gas–liquid drag force. A hydrophilic channel surface could benefit the transport of reactants to the reaction sites, but would also introduce a significantly higher pressure drop. A sharp corner channel could be a better design option since it would provide a space for water accumulation and paths for water to climb onto upper surfaces. Increasing the inlet velocity could facilitate water management, but the corresponding pressure drop was also increased linearly.

Non-uniform flow distribution (maldistribution) in multiple channels is another major concern in channel design. Wang et al. [104] developed a mixture model to simulate the simultaneous flow of liquid water and gaseous reactants in straight minichannels of a PEM fuel cell. The results showed that under fully humidified inlet conditions, liquid water built up quickly at the inlet and was followed by a slow increase downstream. Water was found to stick around the region with a geometrical heterogeneity. They [106] also examined the maldistribution effects in parallel channels of PEM fuel cells, where GDL intrusion into the channels was found to cause severe flow maldistribution. And the intrusion of GDL can be experimentally measured by a method based on residence time distribution in fuel cell flow fields [40]. Employing flow splitters in the inlet manifold can mitigate such flow maldistribution. However, their simulation results were steady-state and isothermal, and droplet formation cannot be captured using this two-phase flow model.

5.2.3. PEM fuel cell performance

The literature discussed above mainly focused on the hydrodynamic behavior of two-phase flow in the gas channel without considering electrochemical reactions. Although these studies can provide a fundamental view of liquid water evolvement into the flow field channel, the lack of reaction makes it difficult to predict the complicated two-phase phenomena happening in a real PEM fuel cell. The non-uniform reaction in the catalyst layer results in a non-uniform water generation rate and thus has a great impact on the subsequent two-phase flow in flow field channels. Meanwhile, non-uniform water distribution in flow field channels also affects the diffusion of reactants, which reduces the PEM fuel cell performance.

A general 3D model of a PEM fuel cell has been developed by Le and Zhou [96], which couples the VOF method with electrochemical reaction, heat transfer, and species transport. Liquid droplets were initially located on the sidewalls of a single serpentine cathode channel and the two-phase flow patterns, effects of channel structure, current density, and temperature distribution were discussed in detail. Furthermore, they applied this model to investigate the flow behavior of liquid water in serpentine-parallel flow channels [97] and in interdigitated flow channels [111]. The results showed that the liquid droplets caused high pressure drop, decreased the local cell temperature, and blocked the pathway of reactants, but the droplets also increased the ionic conductivity of the catalyst layers and the membrane. However, the GDL, catalyst layer, and membrane were all assumed to be homogenous media, and it is not appropriate to apply the VOF method to a homogenous porous region. To improve the cell performance, the flow channel aspect ratio can be modified to increase the sub-rib convection. This increase resulted in higher reactant velocity, faster liquid water removal, and better cell performance [112]. However, excessive sub-rib convection may also dry out the membrane.

Flow maldistribution is an issue in an operating PEM fuel cell, as shown by Basu et al. [105] via an integrated mixture model with electrochemical reactions. The model was validated against experimental data of the wetted area on the GDL surface and pressure drop on the cathode side. The effect of GDL intrusion at the edge channels, which can lead to flow maldistribution, was numerically studied and the results are shown in Fig. 17.

At low flow rates, channel intrusion blocks the GDL surface and makes the edge regions starved of reactants. Innovative flow field designs, such as those developed by Wilkinson et al. [113], are required to mitigate this type of flow maldistribution of gas reactants.

6. Water mitigation strategies

Water in the PEM fuel cell is an unavoidable product of the electrochemical reaction and the presence of local oversaturated water vapor. Therefore, water mitigation, as part of the overall water management, will always be an issue for PEM fuel cells. Even if steps are taken to avoid severe flooding in active fuel cells, considerations need to be given to the increased parasitic power loss associated with implementing water mitigation strategies. The main purposes of these strategies are to maintain a water balance inside the cell and to reduce the damages associated with two-phase flow inside the flow field channels, the gas diffusion layers

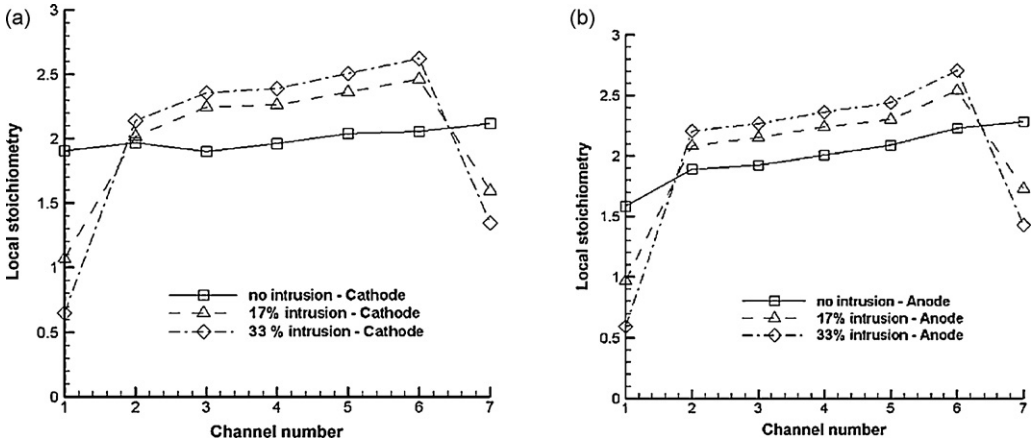

Fig. 17. Plots of local stoichiometry of different channels at different intrusions on (a) cathode and (b) anode sides [105].

(GDLs), and the catalyst layers (CL). Some of the methods used to improve water management are based on simply modifying the operating conditions of the fuel cell, which in part depend on the targeted application. The different components of a fuel cell system can also be individually designed in order to mitigate the overall water management issues. In addition, the use of extra systems or components (e.g., external valves, acoustic woofers, electroosmotic pumps, etc.) has been developed to improve the cell's performance by solving durability issues related to poor water management. However, many water management approaches lead to increased system volume and complexity, so continued study into two-phase flow and its applications to water management is still essential.

6.1. Operating conditions

Modifying the operating conditions in fuel cell systems is a common water mitigation strategy. A key goal for the PEMFC is to keep all water in the vapor state but close to saturation to prevent membrane dehydration. Some of the operating conditions that determine the water accumulation (or water dehydration) inside a fuel cell are gas flow rates, pressures, temperatures, relative humidities, and specific current loads at which the fuel cell is running.

Usually, gas flow rates are based on stoichiometry, which is defined in Eq. (3). Since most of the water is accumulated on the cathode side of the fuel cell, much attention has been paid to the effect of high air/oxygen flow rates on the removal of water. When pure oxygen is used, the required stoichiometry is typically between 1.2 and 1.5, and when air is used the stoichiometry is 2.0 or higher [114]. Higher gas flow rates increase the cell performance, but also increase the total parasitic losses since the air compressor would consume more power [31]. Through the use of a transparent fuel cell, Liu et al. [6,115] observed how the accumulated water droplets and slugs in the flow field channels are removed efficiently when higher air flow rates are used. Although the performance of the cell improves with higher air stoichiometries, excessively high flow rates dry the membrane and the overall voltage decreases significantly. Natarajan and Nguyen [116] demonstrated that high flow rates affect the local current densities and ohmic resistances of the membrane, especially near the inlet of the cathode flow field channel due to membrane dehydration.

The use of high gas flow rates can also be used in order to purge accumulated liquid water inside the channels, the GDL and the membrane. This purging step is especially important when the fuel cell is operated at freezing temperatures, thus, dry gas is used at both reactant streams during the shutdown procedure in order to eliminate most of the liquid water [117–119]. In some cases, avoiding anode purging also helps to improve the overall fuel cell efficiency of the system [117]. One of the parameters that affect the gas purging method is the moment at which it is performed. If the stack is purged right after cell operation, then there is a high probability that a large amount of water will still stay inside the cell after purging. Conversely, if the cell is allowed to cool to room temperature, a greater amount of water will condense and the dry gas can remove it more effectively. Another factor for this process is the purge duration in which the gas purging should be performed at. The resistance of the membrane increases significantly after a specific period of time in which the water near the membrane is evaporated. Ideally, the purge is not performed for extensive periods of time because a dry membrane (high membrane resistance) will have a direct impact on the current that the stack will be able to achieve during the cold startup. Normally, gas purging is performed for not more than a minute [117,120]. One other parameter that can have a direct impact on the stack's performance after purging is the humidity of the purging gas. As stated previously, dry gases are normally used for this procedure, but they can increase the membrane resistance very rapidly. Introducing humidity to the purging has can reduce the degradation of the membrane without significantly affecting the removal of water from the cell [121]. The use of humidity in the purging step becomes even more important after a number of freeze/thaw cycles in order to avoid overall performance degradation [122,123]. Tajiri et al. [124,125] proposed an experimental purging method where a partially humidified gas is introduced to the fuel cell for several hours. Through this method, the water inside the fuel cell evaporates and the water content in the membrane reaches a thermodynamic equilibrium. Thus, the initial water content in the membrane is well defined prior to the cold start tests. It is important to note that this method is intended for laboratory purposes only since it is not realistic in practical applications (increase of parasitic losses). For more information on purging and its influence in cold starts, the reader is recommended to view the following studies [126–129].

The pressure of the gases, the pressure drop within the flow field plates, and the pressure difference between the anode and cathode sides are vital parameters that can be manipulated in order to improve the water removal inside fuel cells (details about flow field designs and their pressure drops are given in Section 6.2.2). Anode water removal, proposed by Ballard Power Systems [130–132], creates a pressure drop between the anode and cathode to modify the water concentration gradient of the proton exchange membrane. This gradient increases the back diffusion rate of water from the cathode towards the anode, reducing the water amount on the cathode side. Although this method can be accomplished by modifying the relative humidity or thermal gradient of the anode side, the

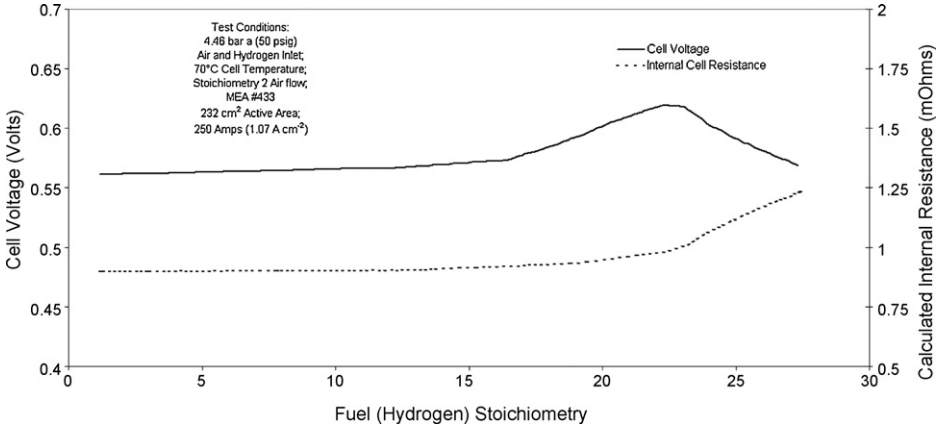

Fig. 18. Example of the improvement of a single cell performance due to the anode water removal method [131].

recommended approach is to create a pressure drop within the cell [131]. The pressure of the anode gas stream decreases along the flow channel at high fuel flow rates (high stoichiometries) of the fuel gas. Once the flow rate reaches an optimum level, the pressure drop draws water from the cathode side towards the anode through the membrane. The cell voltage increases with higher fuel flow rates until a peak in performance is reached (Fig. 18), where the cell's internal resistance increases with high flow rates due to the membrane drying out from too much water removal [131]. A clear advantage of this method, especially if the fuel cell system recycles the hydrogen used, is that it does not increase the parasitic losses involved with the use of high air flow rates. However, one concern with this approach is the possible degradation (and possible rupture) of the membrane caused by the pressure differences between the anode and cathode sides. Another issue with this method is the parasitic losses involved with the increase of hydrogen flow rate and its direct impact on the overall fuel efficiency in the system.

The temperature of the fuel cell has a great effect on the overall cell performance and on the water accumulation inside the flow field channels. At low temperatures, more liquid water accumulates in the channels, which blocks the airflow and decreases the cell's performance due to the lack of oxygen reaching active sites in the catalyst layer. Once the temperature is increased, the amount of liquid water in the channels is reduced since the vapor condensation rate at high temperatures is slower than at low temperatures [115]. Therefore, the flow channels are substantially less blocked with water and the cell's performance improves. In addition, when the cell temperature is increased the cathode pressure drop decreases since there is less liquid water present in the gas diffusion layers and subsequently the flow channels [133]. Chuang et al. [134] observed that even slight changes of the cell temperature (76–80 °C) are enough to decrease the amount of liquid water accumulated in the channels and in the GDLs, especially at high current densities. Higher temperatures also decrease the surface tension and viscosity of liquid water, facilitating more convective water removal in the flow channels [133]. Increasing the temperature between the cathode inlet and outlet to establish a thermal gradient has been shown to be an effect method for water management [135]. This can be accomplished through the use of a coolant flow field that can create such temperature gradients. In addition, temperature gradients can be controlled inside fuel cell stacks in order to improve fuel cell startup from freezing temperatures. Bradean et al. [136] presented a new stack design in which the stack was insulated everywhere except on one stack end, and in the other end a heat reservoir is placed between the stack and the insulation. After shutdown, the heat in the heat reservoir flows through the stack, improving the water mitigation inside the MEAs. In general, the use of temperature gradients in order to control the water migration from one side of the membrane to the other, also referred to as thermo-osmosis, is of critical importance so the overall water issues can be reduced [137,138]. A number of researchers have studied this temperature driven flow, but more work still needs to be performed so it can be fully understood and used efficiently in future fuel cell designs [139,140].

The relative humidity is another important operating condition that can be manipulated to mitigate water flooding and two-phase flow inside fuel cells. Bernardi [141] discussed how the water balance in fuel cells is more sensitive to changes in the relative humidities at the inlet of the air stream than at the inlet of the fuel side, leading most studies to deal with the relative humidity on the cathode side. Büchi and Srinivasan [142] performed tests with dry gases and showed the performance of the cell was lower compared to the same cell with humidified gases. This performance loss was attributed to the increase of the membrane's resistance due to dehydration (and reduced liquid content in the channels and MEA). In general, the ideal relative humidity (if necessary) for a fuel cell system has to be determined based on the flow field design, the MEA materials, and the application in which the fuel cell system will be used. For example, if the GDL does not have enough porosity it may not remove water efficiently at higher water production rates. However, at dry conditions that may be favorable since the water accumulated in the GDL can keep the membrane humidified. Fig. 19 shows an example of a single fuel cell with and without humidified gases. It is evident that at high current densities (greater than 2000 mA cm^{-2}) the membrane is likely dehydrated, causing the cell performance to quickly deteriorate. Although at the mid-range current densities the cell with dry gases performs similarly to the humidified gases, it is important to note that after prolonged hours of operation a number of failures are encountered, which are likely associated with the dry gases (i.e., dehydration due to lack of water content in the fuel cell). In general, there should be a water balance inside the fuel cell, and the ideal humidity for a specific fuel cell design and operating condition(s) should be the one that achieves such balance.

6.2. Fuel cell design

Manipulating the proton exchange membrane, the catalyst layer, the gas diffusion layers, and the flow field channels to improve the overall water management inside fuel cell stacks are all valid water mitigation strategies that have been studied and developed. It is important to note that one main concept that can be implemented in any fuel cell component is based on creating non-uniformity and in-plane gradients in the fuel cell structure in

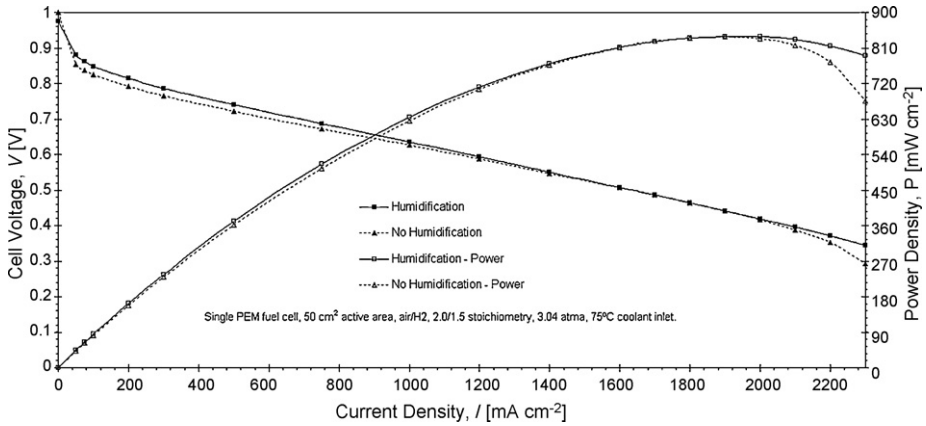

Fig. 19. Comparison between humidified gases (100% relative humidity) and no humidified (dry) gases. The MEA was composed of a Gore 5510 Primea Series membrane (0.4 mg Pt cm^{-2} in each side), SGL 25 BC GDLs for both anode and cathode sides. The active area was 50 cm^2.

order to improve the overall performance of the cell [143]. These gradients along the MEA's surface (or between components) can change the electrochemical activity, or modify the water transport along the whole cell. For example, by creating pressure and/or temperature gradients along the GDLs and the flow field channels (between the inlet and the outlet points of the gas streams) the accumulation of water and subsequent water removal can be significantly improved. Many other parameters can be manipulated non-uniformly such as hydrophobicity (PTFE content) and porosity.

6.2.1. Membrane electrode assembly design

Designing and modifying each component of the MEA is a common strategy to reduce water accumulation and two-phase flow inside the flow field channels and the whole fuel cell. The use of thin membrane materials improves the back diffusion rates of water from the cathode side towards the anode side. However, due to mechanical strength issues the membrane cannot be too thin because pinholes can be formed quickly and the membrane can dry out more quickly. Membranes between 25 and 40 μm in thickness are recommended for most fuel cell applications [144].

One approach to reduce two-phase flow within the cell and channels is to use membranes with porous fiber wicks, as proposed by Watanabe et al. [145]. In this method, twisted threads of porous polyester fibers are coupled to the proton exchange membrane in order to supply water directly to the membrane. Thus, the MEA has less resistance and is fully humidified without the need to humidify the reactant gases prior to entering the cell. They also found that reducing the amount of porous fibers can modify the amount of water supplied through the wicks depending on the current density and fuel cell application.

Catalyst layer structure can also be modified in order to reduce the effect of flooding by improving the gas and liquid water transport [144,146]. Lin and Nguyen [147] proposed a catalyst layer structure that separates transport channels for gas and liquid phases. The structure has a number of ionic (Nafion) and electronic (carbon with catalyst) interconnected paths for proton and electron transport. The ionic film must be thick enough to avoid ionic resistance but thin enough to facilitate gas transport. This structure also has hydrophobic particles (Teflon) filling parts of the empty spaces between the ionic and electronic networks in order to allow gas and liquid transport. Thus, the voids near the ionic film (hydrophilic) help liquid transport and the voids near the Teflon particles help the gas transport. Watanabe et al. [148] developed thin self-humidifying membranes that have highly dispersed nanocrystallites of Pt and oxides (such as TiO_2 or SiO_2). The Pt particles along with the oxides allow the reaction of H_2 and O_2, while keeping the product water on the hygroscopic oxides.

Gas diffusion layers used in PEM fuel cells are normally treated with an agent such as PTFE or fluoroethylenepropylene (FEP) to increase hydrophobicity. For cathode GDLs, this coating is vital since most of the water produced and accumulated inside the cell exits through the cathode side. For the anode GDL, this coating is not as critical but still important when dealing with back diffusion of water and to give more structural strength to the GDL. The appropriate amount of PTFE content should be determined for both the anode and cathode GDLs. The most common loadings of PTFE and FEP are from 5 to 30 wt%. Lin et al. [147] did an extensive study on the effect of the PTFE content on the performance of Toray and SGL SIGRACET carbon fiber papers. It was observed that increasing the hydrophobicity of the GDL enhanced both the gas and water transport when the fuel cell was operated with high levels of humidity. However, excessive amounts of PTFE reduced the amount of hydrophilic pores, deteriorating the water flow out of the catalyst layer and the GDL. Through the use of a transparent fuel cell, Spernjak et al. [12] observed that with treated GDLs the water produced at the cathode side emerged as droplets on the surface of the material over the entire visible area. With the untreated GDLs, water preferred to be in contact with the sidewalls of the channels, and the water formed films and slugs near the walls. This behavior caused greater water management issues and lowered gas transport towards the active areas. A novel method to increase the hydrophobicity of the GDL was presented by Ji et al. [149], in which the water-proof oil dimethyl silicon (DMS) was sprayed onto one of the surfaces of the GDL and then extracted with a water pump from the opposite side, allowing the oil to pass through the pores of the GDL. The material was then heated to remove any solvent residue. It was shown that water management of a fuel cell with these GDLs improved significantly, especially at high current densities and with over humidified conditions [150].

Normally, the hydrophobic content in the GDLs is constant throughout. However, if certain parts of the GDL have different PTFE contents then the water behavior can be manipulated. A method to vary the PTFE content of a GDL was developed by Mathias et al. [150], leaving high and low PTFE particle density regions around the GDL. Another way of manipulating the GDL in order to overcome water issues is by varying the GDL porosity in specific areas [151]. For instance, grooves or holes can be inserted in the carbon fiber paper in areas where water flooding is a major issue [152]. The location and size of the holes depends on the current densities and the other operating conditions at which the fuel cell will be used. Using carbon cloth materials, which are more porous, in locations of greater water flooding and using carbon fiber paper in the remaining active areas can also create differences in GDL porosity.

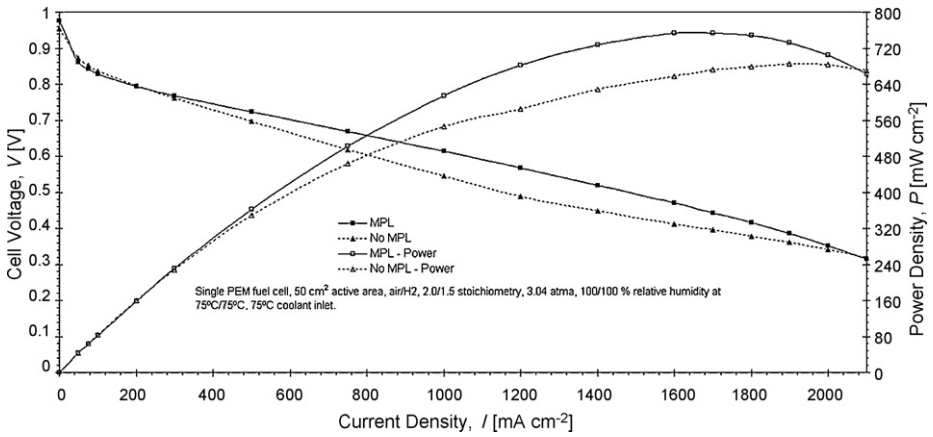

Fig. 20. Comparison between gas diffusion layers (GDLs) with and without micro-porous layers. The MEA was composed of a Gore 5510 Primea Series membrane (0.4 mg Pt cm^{-2} in each side), SGL 25 DC GDL for the anode side, and the cathode GDLs were SGL 25 BC (with MPL) and 25 BA (without MPL). The active area was 50 cm^2.

Another strategy for improving the water transport inside fuel cells is by using a thin micro-porous layer (MPL) on the surface of the GDL that faces the catalyst layer and the membrane. This layer is made with carbon black particles and PTFE (i.e., the layer is hydrophobic), and is usually deposited only on top of one of the GDL surfaces, forming a double-layer diffusion layer. The MPL forms smaller pores and acts as another mechanism to reject water, which is critical when the fuel cell is operated at high humidity levels [153]. Micro-porous layers are now commonly used to improve the overall performance and voltage stability of fuel cells [154]. However, it is still unclear exactly how the MPL affects the water transport mechanism inside the GDL and the MEA. More experimental work is necessary in order to investigate how the MPL helps the performance of the fuel cell [155]. Fig. 20 shows the performance of a fuel cell with and without an MPL on the cathode GDL. It is obvious that at most current densities (and at the peak power density) the MPL has a significant influence on the performance of the cell due to the improved water removal and management.

The hydrophobic particles in the MPL can be distributed along the GDL surface such that certain areas have more (or less) hydrophobicity, creating a gradient that can manipulate the water transport. Chen et al. [155] designed a non-uniform water management layer (or MPL) that was able to keep the relative humidity inside the whole MEA stable within a specific range instead of letting it increase between the inlet and outlet regions. Thus, the proton exchange membrane was kept uniformly hydrated, which resulted in superior performance at high current densities.

6.2.2. Flow field design and configuration

The flow field channels distribute the reactant gases over the electrode surfaces as uniformly as possible in order to utilize as much of the active catalyst area as possible. These channels also have to collect and remove the product water in order to minimize any water flooding. In addition, these flow fields have fixed channel geometries and fixed active areas, which determine the reactant flow characteristics over the operating range of the fuel cell. The most common flow field designs currently in use are parallel (straight) channels, serpentine, and interdigitated [156–159]. The parallel design is made of a number of straight channels connected to common inlet and outlet headers. One issue associated with this design is that water tends to accumulate in the channels and the pressure drop is too low to remove the water [114,157]. This issue leads to the maldistribution of the reactant gases in the flow field, causing reactant starvation in some channels and an excess of reactant in other channels. Serpentine flow fields have one or more continuous channels connected to an inlet and outlet header and typically follow a path with several bends. These flow fields generally have longer channel lengths and a greater pressure drop along the channels due to the bends, which facilitates water removal. Multiple serpentine channels are used for large active areas in order to avoid excessively high pressure drops [158]. Li et al. [160] presented a method for designing serpentine flow fields based on an appropriate flow channel pressure drop so that all of the liquid water is evaporated and removed from the cell through the flow fields. However, it is important to note that the cells designed through this method exhibited inferior performance compared to similar cells found in literature and that the pressure drop can result in a significant parasitic loss for the fuel cell system.

In interdigitated (or discontinuous) flow fields, there are a number of parallel discontinuous channels (i.e., the channels are discontinuous from the inlet header to the outlet header). The reactant gases are forced to flow through the porous electrodes (or GDL) in order to reach the channels connected to the outlet manifolds. Since the gases are forced along a short path through the GDL and catalyst layer, the liquid water is removed more efficiently, resulting in better performance at higher current densities. However, these flow fields do not remove the water located at the inlet of the channels properly, and the voltage stability at low loads (current densities) is very poor [159]. In general, this flow field type is most ideal for high current densities, but it increases the parasitic losses due to the larger pressure drops.

It is important to note that the direction in which the flow fields (coolant included) of a fuel cell are placed also has an influence on the overall water management and performance of the cell. Depending on the application, it may be desirable for the coolest region of the coolant channels to coincide with the area in which the oxygen concentration in the cathode channels is the highest and where there is the least amount of water in the cell. Wilkinson et al. [135] used this approach to create a thermal gradient from cathode inlet to outlet to keep the product water in the vapor phase (see Section 6.1). They also operated a fuel cell with dry gases by using the cathode and coolant flow field in co-flow and the anode in counter-flow. Similarly, cross-flow operation between the fuel and the oxidant channels may be preferred to co-flow or counter-flow configurations (see Fig. 21).

The use of porous plates with standard flow fields has improved water management in fuel cells, especially when dealing with dry conditions and gases at ambient pressures [161]. United Technologies Company (UTC) developed a fuel cell stack with porous bipolar plates in which the pores are filled with liquid water [162–165]. These plates have coolant flow fields filled with water on one side and gas flow channels on the other that are in contact with the MEA. Since the plates are gas impermeable, the gas does not dif-

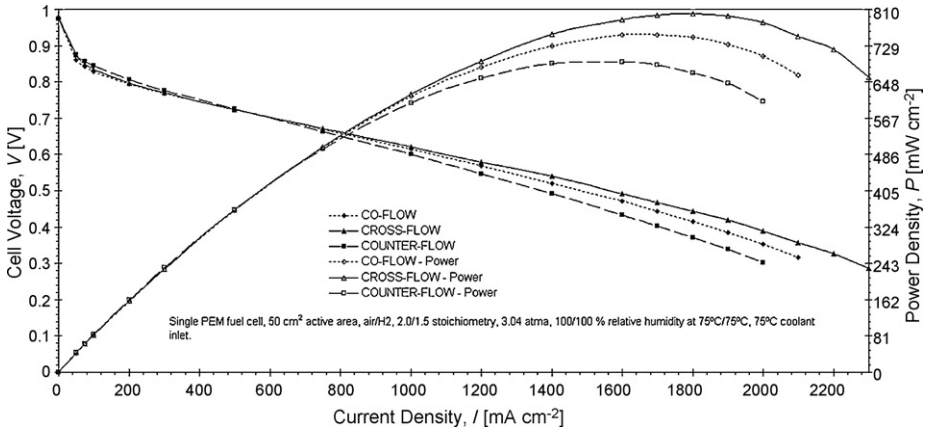

Fig. 21. Comparison between co-flow, cross-flow and counter-flow configurations between the anode and cathode flow fields. The MEA was composed of a Gore 5510 Primea Series membrane (0.4 mg Pt cm^{-2} in each side), SGL 25 DC GDL for the anode and SGL 25 BC GDL for the cathode. The active area was 50 cm^2.

fuse through the pores towards the coolant channels. The water accumulated in the gas channels is wicked towards the coolant side since the gas streams are at higher pressure than the coolant streams. Thus, issues related to water accumulation in the flow field channels are reduced significantly. Miachon and Aldebert [166] also used a porous plate to improve water management by forcing the stack gases to pass through porous carbon blocks situated between non-porous graphite plates in order to reach the GDL instead of flowing through channels.

Another way to modify the flow field channels to reduce the accumulation of water in the GDL and in the flow channels is through the use of absorbent wicking materials. Examples of these materials include polyvinyl alcohol sponges, absorbent cotton cloth, and absorbent cotton paper [167,168]. These wicks can be located near the inlet and outlet areas of the flow field in order to absorb excess water and to humidify the dry gases that enter the channels, which eliminates the need for a humidification system. In a similar method, Sugiura et al. [17] used porous stainless steel sheets as water adsorption layers that were located between the MEA and the flow field channels. Although the water accumulation in the channels was reduced with these layers, the overall ohmic resistance increased, resulting in no overall improvement in the cell's performance.

The cross-sectional shape of the flow field channels also plays a key role in the effective water removal inside the flow field plates. For example, Trabold et al. [169,170] demonstrated how triangular shaped flow field channels can have designated localized water collection regions. The water then accumulates away from the gas diffusion layer, which allows more gas to reach the catalyst layer. In addition, the cross-section of the channels can be designed to change gradually along the length of the channel, modifying the pressure drop and gas distribution along the active area [171]. Johnson et al. [172] developed a differential pressure flow field for water removal by changing the shape of the flow field channels with respect to each other. In micro-fuel cells, Metz et al. [173,174] developed a passive water management system by using capillary microstructures as flow field channels in the cathode plate. These channels are hydrophilic with a tapered cross-section, allowing them to remove liquid water from the GDL towards the cathode plate and a layer of non-woven material.

The flow field channels can also be modified with respect to their hydrophobicity. Hydrophilic channels may improve the transport of gases to the reactant sites by facilitating the water transport in the edges and surfaces of the channels [100]. However, very hydrophilic channels result in greater pressure drops due to liquid water blockage. The wetting capabilities of the channels can be modified by using different cross-sectional geometries or by altering the surface characteristics of the bipolar plate materials [175].

6.3. Additional systems

There have been a number of proposed systems that attempt to improve overall fuel cell stack performance without increasing the parasitic energy demand. Nguyen et al. [176,177] presented a system that used sequential exhaust or purging of individual cells in a stack as a liquid water management strategy. This system used a device (electromechanical valves or rotating device located outside the stack) that allowed each cell in the stack to exhaust separately from the other cells. Thus, each cell was guaranteed to receive adequate gas flow without water accumulation. This system has also been used for larger active area stacks using air instead of oxygen on the cathode side [178]. One important issue with this concept is the added complexity to the system due to the addition of extra valves. Matsumoto et al. [179] proposed a fuel cell stack that changed the flow field of the cathode plates by changing the external port arrangement with valves depending on the power that the cell was working at (i.e., parallel flow field at high power levels and serpentine flow field at low power levels).

Most flow fields are designed to perform well at their peak power point. However, at low current loads fuel cells typically have voltage instability, which is particularly problematic when interdigitated flow fields are used. Therefore, Wilkinson et al. [180,181] developed an approach to change the flow field active area within a cell with changing operations. Novel cathode flow fields were divided into sections, with each unit connected to a valve at the exit of the flow field. When these valves were closed, the outlet of the corresponding section was blocked, forcing the reactant to go to the other sections of the cathode that were still open. Through this method, the water management and voltage stability in single cells and stacks were significantly improved at low current loads and low stoichiometries. This method can also be implemented with micro-valves inside the fuel cell without increasing the overall parasitic losses considerably. A downfall to this method is that by adding the micro-valves in order to control the active area of the cells inside the stack, the complexity of the overall system is significantly increased. In addition to this, the overall reliability of the system is also compromised.

Researchers at Stanford University have designed and developed a PEM fuel cell integrated with an electroosmotic pump to improve the water management of the cells at different conditions [182–186]. In the latest design, a porous carbon plate with

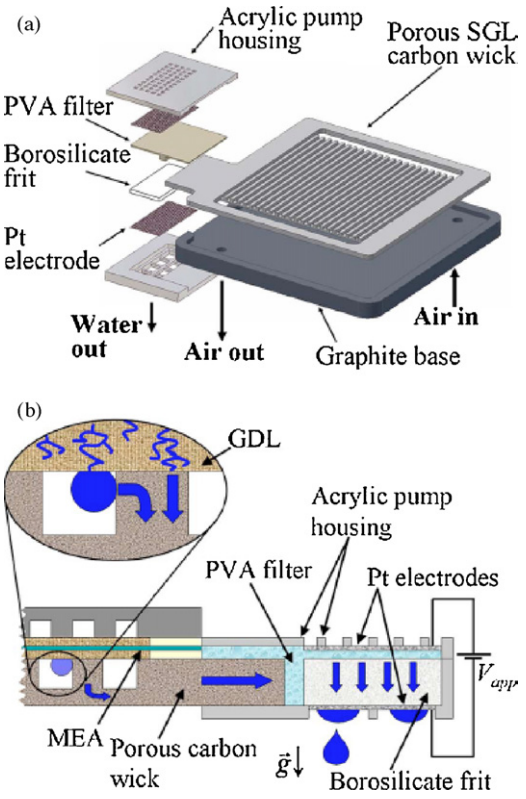

Fig. 22. (a) Schematic of a porous plate with an external electroosmotic pump used in fuel cells and (b) detailed view of the water path with the porous plate and electroosmotic pump [185].

parallel flow field channels was connected to a small electroosmotic pump placed outside the fuel cell. The hydrophilic porous plate acts as a wick and absorbs water from the flow channels and the GDL until the region is saturated. At this point, the pump is used to remove the remaining water from the cell. Between the plate and the pump, there is a polyvinyl alcohol filter that connects both components and filters out any particles that may damage the pump (see Fig. 22). It is claimed that this system consumes just 1% of the overall fuel cell power at low current loads and only up to 0.5% at medium to high current densities. These tests were performed with single cell fuel cells, and the implementation of such a system into an actual fuel cell stack has not been demonstrated. The addition of an electroosmotic pump does not just increase the overall complexity and size of a fuel cell stack, but it can also impose a negative effect towards the overall reliability of the system.

The use of acoustic woofers in order to generate pulsating flows in fuel cells has resulted in the improvement of water management and of the overall performance [187]. However, the overall fuel cell efficiency is slightly decreased due to the use of the woofer. Vibration and acoustic methods have also been considered as possible approaches for the removal of excess product water in PEM fuel cell stacks [188,189]. This method would use waves (flexural, acoustic, or surface waves) to remove the water droplets inside the fuel cell. Unfortunately, these methods are still in the theoretical and modeling stages, and no practical experiments have been reported.

Although most of these systems and approaches have been proven to be effective in improving the water management issues in fuel cells, there are still issues that impede their implementations in larger fuel cell stacks. One such issue is their added complexity, which may be especially challenging for the implementation of control systems.

7. Summary and outlook

Summaries and an outlook for each major theme of this review are covered below. The final remarks provide an overall outlook for how these major pieces fit together.

7.1. Experimental visualization techniques

Visualization cells allow an observer to see the liquid water form and serve as a basis for understanding and characterizing two-phase flow in fuel cells. However, the results are often mainly specific to a given system and flow characteristics are sensitive to specific materials used. The specific contact angles for the flow field plate, GDL material, and transparent plate of a visualization cell are dissimilar to those in a typical graphite bipolar plate fuel cell. Since surface properties are important to two-phase flow on this scale, the specificity of the results must be considered. Therefore, there is a need of method cross-validation. Steps should be taken, perhaps through dimensionless correlations, to make the results of these novel systems applicable to other fuel cells.

7.2. In situ experimental two-phase flow studies in PEM fuel cells

In situ studies have covered a wide range of variables including the PTFE content of the GDL, the inclusion of an MPL, flow field design, reactant gas stoichiometry, gas relative humidity, and temperature. While the influence of these parameters on fuel cell performance has been well documented, less attention has been paid to the flow field channel hydrodynamics. Thorough analysis of the channel hydrodynamics is still lacking in terms of two-phase flow regimes, two-phase flow distribution, and two-phase pressure drop. These studies are important because the flow regime affects the nature of the water and access of reactant to the catalyst sites, and large two-phase pressure drop represents a parasitic power loss to fuel cell operation. Furthermore, flow maldistribution must be considered as some flow field channels may receive insufficient reactant for the electrochemical reaction, causing starvation and underutilization of the active catalyst area. Hydrodynamics will thus play an increasingly important role in PEM fuel cell water management studies.

7.3. Ex situ experimental two-phase flow studies in PEM fuel cells

The current ex situ experimental studies have been carried out to understand flow distributions, pressure drop, flow patterns, droplet formation, and water removal in flow field channels under flow conditions relevant to fuel cell operation. In the literature, typical two-phase flow patterns found in ex situ experiments are slug flow, slug to stratified flow, and stratified/annular flow. Among those, stratified flow or annular flow is desirable in terms of water management and operating stability of an active fuel cell. Slug flow should be avoided in operation since it can lead to channel blockage and flooding as well as current and pressure fluctuations. Therefore, high gas stoichiometry is required to achieve the desired flow pattern. Flow instability, flow maldistributions, and flow hysteresis have been found in both ex situ and in situ studies on two-phase flow in parallel channels due to many factors such as channel geometry, intrusion of the compressed GDL in channels, and gas/liquid flow rates. In order to achieve even flow distribution and to overcome flow hysteresis phenomena, high gas velocities are desirable. However, high gas flows are not desirable in practical systems because of the parasitic power loss.

There has been some success in obtaining information on instantaneous gas flow rates in individual channels through an entrance pressure drop measurement technique. However, extensive studies are still required to be related to a broader range of operating

conditions such as channel dimensions, gas and liquid flow rates (corresponding to current density and gas stoichiometry), and channel surface properties. In addition, a theoretical foundation to elucidate flow distribution in parallel channels is still lacking, especially for two-phase flow.

A unique aspect of two-phase flow phenomena in fuel cell flow fields is that the liquid water emerges from porous GDLs and accumulates along the flow channels. Therefore, the two-phase flow patterns and pressure drop of such flow systems are likely not accurately predicted by most of the existing correlations or models. Consequently, these correlations should be revisited for two-phase flow in the fuel cell.

7.4. Numerical simulations

PEM fuel cell modeling has undergone remarkable progress in recent years. Comprehensive CFD models are powerful tools in PEM fuel cell modeling due to their easy implementation and their capability to couple with other sophisticated models. However, these numerical tools remain limited for several reasons.

Modeling two-phase flow in PEM fuel cell is still challenging work due to the diverse length scales (from nanometer to meter). A macroscopic two-phase flow model such as the VOF method, which is able to capture the droplet's dynamic behaviors, requires explicit wall position information. However, fully considering electrode microstructure is almost impossible at this point due to the large computational time involved. Instead, the homogenous assumption is always used in simulation, which to some extent lacks precision because of empirical material and transport properties. On the other hand, a microscopic model such as the LBM method is useful in modeling these properties in porous media, but it is quite difficult to extend its application to large-scale simulations such as a PEM fuel cell unit. Multi-scale strategies are required to consider both micro- and macroscopic effects. As computational capabilities increase, it is evident that the gap between microscopic models and macroscopic models will become smaller and smaller.

The coupling of complicated two-phase models with electrochemical reactions and heat transport and associated experimental validation is required. This remains challenging work due to the different length and time scales between simulations and the lack of experimental data. Thus, more fundamental work is needed and more criteria should also be developed to allow for a comprehensive evaluation of two-phase models.

7.5. Water mitigation strategies

In order to avoid or reduce water management issues inside the fuel cell, a number of water mitigation strategies have been developed. Some of these methods consist of varying the operating conditions of the fuel cell (e.g., temperature, pressure, relative humidities, etc.) or designing the different components inside the cell for water management. For example, the flow field channels of cathode bipolar plates can be designed to improve how water is removed inside the channels and the GDL. Similarly, the membrane, catalyst layer, and GDLs can all be specifically designed to improve water management.

Unfortunately, there are no water mitigation methods to date that can deal with water management effectively without affecting other components, especially the membrane and catalyst layers. Thus, more research has to be performed in order to achieve ideal designs and mitigation strategies specific for certain operating conditions and fuel cell applications.

7.6. Overall outlook

Water management studies are shifting from parametrically based studies that couple water behavior with overall fuel cell performance to specific studies on water management in the catalyst layer, GDL, and gas flow channels. These more specific studies provide an understanding of the hydrodynamics in a fuel cell. To study the two-phase flow in PEM fuel cell flow channels, work must continue in all of the previously discussed major areas: ex situ approaches, in situ testing, and numerical simulations. A combined effort of ex situ and in situ experiments can help to validate current numerical simulations and help numerical simulations more accurately reflect the actual two-phase flow phenomena that occur in fuel cells. A greater understanding of two-phase flows experimentally and numerically will allow more effective water mitigation strategies to be developed and implemented in practice. Specific areas that need to be better understood include work on hydrodynamics of two-phase flow in gas flow channels such as flow patterns, pressure drops, flow maldistribution, and flow hysteresis under conditions of great relevance to fuel cell operation. In addition, underlying theoretical foundations should be developed to guide fuel cell flow field design and operation from two-phase flow perspectives. Regarding two-phase flow modeling, an integrated multi-scale approach to model water transports from its formation on the MEA surface to condensation and accumulation in GDL and gas channels and removal from the gas channel will be desirable due to limited computational facility available. Improvements in these areas will eventually lead to higher overall PEM fuel cell performance and efficiency, making the PEM fuel cell a more viable technology for the future.

Acknowledgement

The authors are grateful to a strategic grant from the Natural Sciences and Engineering Research Council of Canada (NSERC) to support this work.

References

[1] H. Li, Y. Tang, Z. Wang, Z. Wang, Z. Shi, S. Wu, D. Song, J. Zhang, K. Fatih, J. Zhang, H. Wang, Z. Liu, R. Abouatallah, A. Mazza, J. Power Sources 178 (2008) 103–117.
[2] T.A. Trabold, Heat Transfer Eng. 26 (2005) 3–12.
[3] T.E. Springer, T.A. Zawodzinski, S. Gottesfeld, J. Electrochem. Soc. 138 (8) (1991) 2334–2342.
[4] D.M. Bernardi, M.W. Verbrugge, AIChE J. 37 (8) (1991) 1151–1163.
[5] F.Y. Zhang, X.G. Yang, C.Y. Wang, J. Electrochem. Soc. 153 (2006) A225–A232.
[6] X. Liu, H. Guo, F. Ye, C.F. Ma, Int. J. Hydrogen Energy 33 (2008) 1040–1051.
[7] T. Ous, C. Arcoumanis, J. Power Sources 173 (2007) 137–148.
[8] H. Masuda, K. Ito, T. Oshima, K. Sasaki, J. Power Sources 177 (2008) 303–313.
[9] K. Tüber, D. Pocza, C. Hebling, J. Power Sources 124 (2003) 403–414.
[10] A. Hakenjos, H. Muenter, U. Wittstadat, C. Hebling, J. Power Sources 131 (2004) 213–216.
[11] F.-B. Weng, A. Su, C.Y. Hus, C.-Y. Lee, J. Power Sources 157 (2006) 674–680.
[12] D. Spernjak, A.K. Prasad, S.G. Advani, J. Power Sources 170 (2007) 334–344.
[13] S. Ge, C.Y. Wang, J. Electrochem. Soc. 154 (2007) B998–B1005.
[14] A. Theodorakakos, T. Ous, M. Gavaises, J.M. Nouri, N. Nikolopoulos, H. Yanagihara, J. Colloid Interface Sci. 300 (2006) 673–687.
[15] R. Shimoi, M. Masuda, K. Fushinobu, Y. Kozawa, K. Okazaki, Trans. ASME 126 (2004) 258–261.
[16] H.-S. Kim, T.-H. Ha, S.-J. Park, K. Min, M. Kim, Proceedings of the 3rd International Conference on Fuel Cell Science Engineering and Technology, Ypsilanti, USA, 2005, pp. 57–63.
[17] K. Sugiura, M. Nakata, T. Yodo, Y. Nishiguchi, M. Yamauchi, Y. Itoh, J. Power Sources 145 (2005) 526–533.
[18] H.P. Ma, H.M. Zhang, J. Hu, Y.H. Cai, B.L. Yi, J. Power Sources 162 (2006) 469–473.
[19] X.G. Yang, F.Y. Zhang, A.L. Lubawy, C.Y. Wang, Electrochem. Solid-State Lett. 7 (2004) A408–A411.
[20] M. Wang, H. Guo, G. Ma, J. Power Sources 257 (2006) 181–187.
[21] J. Cho, H.-S. Kim, K. Min, J. Power Sources 185 (2008) 118–128.
[22] P. Chang, J. St-Pierre, J. Stumper, B. Wetton, J. Power Sources 162 (2006) 340–355.
[23] J. St-Pierre, J. Electrochem. Soc. 154 (2007) B724–B731.
[24] J.P. Owejan, T.A. Trabold, D.L. Jacobson, M. Arif, S.G. Kandilkar, G. Satsih, Proceedings of the Fifth International Conference on Nanochannels Microchannels and Minichannels, Puebla, Mexico, June, 2007, pp. 401–408.
[25] M.A. Hickner, N.P. Siegel, K.S. Chen, D.N. McBrayer, D.S. Hussey, D.L. Jacobson, M. Arif, J. Electrochem. Soc. 153 (2006) A902–A908.

[26] Z. Dunbar, R. Masel, J. Power Sources 182 (2008) 76–82.
[27] A. Bazylak, Int. J. Hydrogen Energy 34 (2009) 3845–3857.
[28] S.G. Kandlikar, Heat Transfer Eng. 29 (7) (2008) 575–587.
[29] W. Dai, H. Wang, X.-Z. Yuan, J. Martin, D. Yang, J. Qiao, J. Ma, Int. J. Hydrogen Energy 34 (2009) 9461–9478.
[30] I.S. Hussaini, C.-Y. Wang, J. Power Sources 187 (2) (2009) 444–451.
[31] D.P. Wilkinson, H.H. Voss, K. Prater, J. Power Sources 49 (1994) 117–127.
[32] S.-S. Hsieh, Y.-J. Huang, B.-S. Her, Int. J. Heat Mass Transfer 52 (2009) 5657–5659.
[33] X. Liu, H. Guo, F. Ye, C.F. Ma, Electrochim. Acta 52 (11) (2006) 3607–3614.
[34] K. Ito, K. Ashikaga, H. Masuda, T. Oshima, Y. Kakimoto, K. Sasaki, J. Power Sources 175 (2008) 732–738.
[35] F. Barbir, H. Gorgun, X. Wang, J. Power Sources (2005) 96–101.
[36] P. Rodatz, F. Buchi, C. Onder, L. Guzzella, J. Power Sources 128 (2004) 208–217.
[37] Al-Baghdadi, Al-Janabi, Int. J. Hydrogen Energy 32 (2007) 4510–4522.
[38] S.D. Knights, K.M. Colbow, J. St-Pierre, D.P. Wilkinson, J. Power Sources 127 (2004) 127–134.
[39] J.P. Mayers, R.M. Darling, J. Electrochem. Soc. 153 (2006) A1432–A1442.
[40] J. St-Pierre, A. Wong, J. Diep, D. Kiel, J. Power Sources 164 (2007) 196–202.
[41] L.F. Zhang, W. Du, H.T. Bi, D.P. Wilkinson, J. Stumper, H.J. Wang, J. Power Sources 189 (2009) 1023–1031.
[42] S.G. Kandlikar, Z. Lu, W.E. Domigan, A.D. White, M.W. Benedict, Int. J. Heat Mass Transfer 52 (2009) 1741–1752.
[43] J.S. Allen, ECS Trans. 3 (1) (2006) 1197–1206.
[44] M.J. English, S.G. Kandlikar, Heat Transfer Eng. 27 (4) (2006) 99–109.
[45] E.S. Lee, C. Hidrovo, K. Goodson, J. Eaton, Proceedings of the 6th International Conference on Multiphase Flow, Leipzig, Germany, July, 2007, Paper No. S7_Thu_A_46.
[46] L.F. Zhang, H.T. Bi, D.P. Wilkinson, J. Stumper, H.J. Wang, J. Power Sources 183 (2) (2008) 643–650.
[47] Z. Lu, S.G. Kandlikar, C. Rath, M. Grimm, W. Domigan, A.D. White, M. Hardbarger, J.P. Owejan, T.A. Trabold, Int. J. Hydrogen Energy 34 (2009) 3445–3456.
[48] K. Pehlivan, I. Hassan, M. Vaillancourt, Appl. Therm. Eng. 26 (2006) 1506–1514.
[49] M.K. Akbar, D.A. Plummer, S.M. Ghiaasiaan, Int. J. Multiphase Flow 29 (2003) 855–865.
[50] K.A. Triplett, S.M. Ghiaasiaan, S.I. Abdel-Khalik, D.L. Sadowski, Int. J. Multiphase Flow 25 (1999) 377–394.
[51] J.L. Xu, P. Cheng, T.S. Zhao, Int. J. Multiphase Flow 25 (1999) 411–432.
[52] A. Marchitto, F. Devia, M. Fossa, G. Guglielmini, C. Schenone, Int. J. Multiphase Flow 34 (2008) 128–144.
[53] Y. Taitel, L. Pustylnik, M. Tshuva, D. Barnea, Int. J. Multiphase Flow 29 (2003) 1193–1202.
[54] M. Tshuva, D. Barnea, Y. Taitel, Int. J. Multiphase Flow 25 (1999) 1491–1503.
[55] G. Hetsroni, A. Mosyak, Z. Segal, E. Pogrebnyak, Int. J. Multiphase Flow 29 (2003) 341–360.
[56] L. Pustylnik, D. Barnea, Y. Taitel, AIChE J. 52 (2006) 3345–3352.
[57] C. Schillberg, S. Kandlikar, Proceedings of the Fifth International Conference on Nanochannels Microchannels and Minichannels, Puebla, Mexico, June, 2007, pp. 299–310.
[58] E.C. Kumbur, K.V. Sharp, M.M. Mench, J. Power Sources 161 (2006) 333–345.
[59] J. Borrelli, T. Trabold, S. Kandlikar, J. Owejan, Proceedings of the Third Annual Conference on Microchannels and Minichannels', 2005.
[60] E. Kimball, T. Whitaker, Y. Kevrekidis, J. Benziger, AIChE J. 54 (2008) 1313–1332.
[61] T. Murahashi, H. Kobayashi, E. Nishiyama, J. Power Sources 175 (2008) 98–105.
[62] J. Wu, X.Z. Yuan, J.J. Martin, H. Wang, J. Zhang, H. Shen, S. Wu, W. Merida, J. Power Sources 184 (2008) 104–119.
[63] Z. Lu, A.D. White, J. Pelaez, M. Hardbarger, W. Domigan, J. Sergi, S.G. Kandlikar, Proceedings of the Sixth International ASME Conference on Nanochannels Microchannels and Minichannels, June 23–25, 2008.
[64] P. Concus, R. Finn, Appl. Math. Sci. 63 (1969) 292–299.
[65] A. Bazylak, J. Heinrich, N. Djilali, D. Sinton, J. Power Sources 185 (2) (2008) 1147–1153.
[66] C. Fang, C. Hidrovo, F.-M. Wang, J. Eaton, K. Goodson, Int. J. Multiphase Flow 34 (2008) 690–705.
[67] E. Shirani, S. Masoomi, J. Fuel Cell Sci. Technol. 5 (4) (2008) 041008–41018.
[68] P. Young, T. Brackbill, S. Kandlikar, Proceedings of the Fifth International Conference on Nanochannels Microchannels and Minichannels, Puebla, Mexico, June, 2007, pp. 827–836.
[69] S. Kandlikar, S. Joshi, S. Tian, Heat Transfer Eng. 24 (3) (2003) 4–16.
[70] A.Z. Weber, J. Newman, Chem. Rev. 104 (10) (2004) 4679–4726.
[71] C.Y. Wang, Chem. Rev. 104 (10) (2004) 4727–4765.
[72] A. Biyikoglu, Int. J. Hydrogen Energy 30 (11) (2005) 1181–1212.
[73] W.Q. Tao, C.H. Min, X.L. Liu, Y.L. He, B.H. Yin, W. Jiang, J. Power Sources 160 (1) (2006) 359–373.
[74] N. Djilali, P.C. Sui, Int. J. Comput. Fluid Dynam. 22 (1–2) (2008) 115–133.
[75] C. Siegel, Energy 33 (9) (2008) 1331–1352.
[76] J.J. Baschuk, X. Li, J. Power Sources 86 (1–2) (2000) 181–196.
[77] D. Natarajan, T. Van Nguyen, J. Electrochem. Soc. 148 (12) (2001) A1324–A1335.
[78] T. Berning, N. Djilali, J. Electrochem. Soc. 150 (12) (2003) A1589–A1598.
[79] S. Litster, N. Djilali, in: B. Sunden, M. Faghri (Eds.), Transport Phenomena in Fuel Cells, WIT Press, 2005, pp. 175–213.
[80] Z.H. Wang, C.Y. Wang, K.S. Chen, J. Power Sources 94 (1) (2001) 40–50.
[81] V. Gurau, R.V. Edwards, J.A. Mann, T.A. Zawodzinski, Electrochem. Solid-State Lett. 11 (8) (2008) B132–B135.
[82] C.Y. Wang, Electrochem. Solid-State Lett. 12 (2) (2009) S2–S3.
[83] V. Gurau, Electrochem. Solid-State Lett. 12 (2) (2009) S4–S6.
[84] C.W. Hirt, B.D. Nichols, J. Comp. Phys. 39 (1) (1981) 201–225.
[85] P. Quan, B. Zhou, A. Sobiesiak, Z. Liu, J. Power Sources 152 (2005) 131–145.
[86] H. Chen, S. Chen, W. Matthaeus, Phys. Rev. A 45 (1992) R5339–R5342.
[87] K.S. Chen, M.A. Hickner, D.R. Noble, Int. J. Energy Res. 29 (12) (2005) 1113–1132.
[88] K.S. Chen, ECS Trans. 11 (1) (2007) 715–724.
[89] G. He, P. Ming, Z. Zhao, A. Abudula, Y. Xiao, J. Power Sources 163 (2) (2007) 864–873.
[90] Z. Zhan, J. Xiao, M. Pan, R. Yuan, J. Power Sources 160 (1) (2006) 1–9.
[91] Y.H. Cai, J. Hu, H.P. Ma, B.L. Yi, H.M. Zhang, J. Power Sources 161 (2) (2006) 843–848.
[92] X. Zhu, P.C. Sui, N. Djilali, J. Power Sources 172 (1) (2007) 287–295.
[93] A. Bazylak, D. Sinton, N. Djilali, J. Power Sources 176 (1) (2008) 240–246.
[94] X. Zhu, P.C. Sui, N. Djilali, Microfluid. Nanofluid. 4 (6) (2008) 543–555.
[95] X. Zhu, P.C. Sui, N. Djilali, J. Power Sources 181 (1) (2008) 101–115.
[96] A.D. Le, B. Zhou, J. Power Sources 182 (1) (2008) 197–222.
[97] A.D. Le, B. Zhou, Electrochim. Acta 54 (8) (2009) 2137–2154.
[98] K. Jiao, B. Zhou, P. Quan, J. Power Sources 154 (1) (2006) 124–137.
[99] K. Jiao, B. Zhou, P. Quan, J. Power Sources 157 (1) (2006) 226–243.
[100] P. Quan, M.C. Lai, J. Power Sources 164 (1) (2007) 222–237.
[101] K. Jiao, B. Zhou, J. Power Sources 169 (2) (2007) 296–314.
[102] K. Jiao, B. Zhou, J. Power Sources 175 (1) (2008) 106–119.
[103] L. Hao, P. Cheng, J. Power Sources 186 (1) (2009) 104–114.
[104] Y. Wang, S. Basu, C.Y. Wang, J. Power Sources 179 (2) (2008) 603–617.
[105] S. Basu, J. Li, C.Y. Wang, J. Power Sources 187 (2) (2009) 431–443.
[106] S. Basu, C.Y. Wang, K.S. Chen, J. Fuel Cell Sci. Technol. 6 (3) (2009), 031007-1–031007-11.
[107] S. Um, C.Y. Wang, K.S. Chen, J. Electrochem. Soc. 147 (12) (2000) 4485–4493.
[108] S. Mazumder, J.V. Cole, J. Electrochem. Soc. 150 (11) (2003) A1503–A1509.
[109] X. Zhu, Q. Liao, P.C. Sui, N. Djilali, J. Power Sources 195 (3) (2010) 801–812.
[110] Y. Ding, H.T. Bi, D.P. Wilkinson, J. Stumper, H.J. Wang, Proceedings of the 20th International Symposium on Transport Phenomena, Victoria, Canada, 2009.
[111] A.D. Le, B. Zhou, J. Power Sources 193 (2) (2009) 665–683.
[112] X.D. Wang, Y.Y. Duan, W.M. Yan, D.J. Lee, A. Su, P.H. Chi, J. Power Sources 193 (2) (2009) 684–690.
[113] D.P. Wilkinson, O. Vanderleeden, J. Zimmerman, US6,541,145 (2003).
[114] F. Barbir, PEM Fuel Cells: Theory and Practice, Elsevier Academic Press, New York, 2005, pp. 119–121.
[115] X. Liu, H. Guo, C.F. Ma, J. Power Sources 156 (2006) 267–280.
[116] D. Natarajan, T.V. Nguyen, AIChE J. 51 (2005) 2587–2598.
[117] J. St-Pierre, J. Roberts, K. Colbow, S. Campbell, A. Nelson, J. New Mater. Electrochem. Syst. 8 (2005) 163–176.
[118] N.J. Fletcher, G.A. Boehm, E.G. Pow, US5,798,186 (1998).
[119] J.A. Roberts, J. St-Pierre, M.E. Van der Geest, A. Atbi, N.J. Fletcher, US6,479,177 (2002).
[120] K. Tajiri, C.Y. Wang, Y. Tabuchi, Electrochim. Acta 53 (2008) 6337–6343.
[121] K.T. Cho, A. Turhan, J.H. Lee, J.S. Brenizer, A.K. Heller, L. Shi, M.M. Mench, Nucl. Instrum. Methods Phys. Res. A 605 (2009) 119–122.
[122] J. Hou, H. Yu, S. Zhang, S. Sun, H. Wang, B. Yi, P. Ming, J. Power Sources 162 (2006) 513–520.
[123] J. Hou, H. Yu, B. Yi, Y. Xiao, H. Wang, S. Sun, P. Ming, Electrochem. Solid-State Lett. 10 (2007) B11–B15.
[124] K. Tajiri, Y. Tabuchi, C.Y. Wang, J. Electrochem. Soc. 154 (2007) B147–B152.
[125] K. Tajiri, Y. Tabuchi, F. Kagami, S. Takahashi, K. Yoshizawa, C.Y. Wang, J. Power Sources 165 (2007) 279–286.
[126] X. Yu, M. Pingwen, H. Ming, Y. Baolian, Z.G. Shao, J. Power Sources 188 (2009) 163–169.
[127] J.P. Owejan, J.J. Gagliardo, S.R. Falta, T.A. Trabold, J. Electrochem. Soc. 156 (2009) B1475–B1483.
[128] J.P. Owejan, J.J. Glagiardo, J.M. Sergi, S.G. Kandlikar, T.A. Trabold, Int. J. Hydrogen Energy 34 (2009) 3436–3444.
[129] E.A. Cho, J.J. Ko, H.Y. Ha, H.Y. Ha, S.A. Hong, K.Y. Lee, T.W. Lim, I.H. Oh, J. Electrochem. Soc. 151 (2004) A661–A665.
[130] D.P. Wilkinson, H.H. Voss, D.S. Watkins, K.B. Prater, US5,366,818 (1994).
[131] H.H. Voss, D.P. Wilkinson, P.G. Pickup, M.C. Johnson, V. Basura, Electrochim. Acta 40 (1995) 321–328.
[132] H.H. Voss, D.P. Wilkinson, D.S. Watkins, US5,441,819 (1995).
[133] W. He, G. Lin, T.V. Nguyen, AIChE J. 49 (2003) 3221–3228.
[134] P.A. Chuang, A. Turhan, A.K. Keller, J.S. Brenizer, T.A. Trabold, M.M. Mench, Proceedings of Fuel Cell 2005—3rd International Conference of Fuel Cell Science Engineering and Technology, 2005, pp. 31–37.
[135] D.P. Wilkinson, H.H. Voss, N.J. Fletcher, M.C. Johnson, E.G. Pow, US5,773,160 (1998).
[136] R. Bradean, H. Haas, K. Eggen, C. Richards, T. Vrba, ECS Trans. 3 (2006) 1159–1168.
[137] R. Zaffou, J.S. Yi, H.R. Kunz, J.M. Fenton, Electrochem. Solid-State Lett. 9 (2006) A418–A422.
[138] J.P.G. Villaluenga, B. Seoane, V.M. Barragan, C. Ruiz-Bauza, J. Membr. Sci. 274 (2006) 116–122.
[139] S. Kim, M.M. Mench, J. Electrochem. Soc. 156 (2009) B353–B362.
[140] S. Kim, M.M. Mench, J. Membr. Sci. 328 (2009) 113–120.
[141] D.M. Bernardi, J. Electrochem. Soc. 137 (1990) 3344–3350.

[142] F.N. Buchi, S. Srinivasan, J. Electrochem. Soc. 144 (1997) 2767–2772.
[143] D.P. Wilkinson, J. St-Pierre, J. Power Sources 113 (2003) 101–108.
[144] T.V. Nguyen, ECS Trans. 3 (2006) 1171–1180.
[145] M. Watanabe, Y. Satoh, C. Shimura, J. Electrochem. Soc. 140 (1993) 3190–3193.
[146] T.V. Nguyen, D. Natarajan, R. Jain, ECS Trans. 1 (2005) 501–508.
[147] G.Y. Lin, T.V. Nguyen, J. Electrochem. Soc. 152 (2005) A1942–A1948.
[148] M. Watanabe, H. Uchida, Y. Seki, M. Emori, P. Stonehart, J. Electrochem. Soc. 143 (1996) 3847–3852.
[149] M.B. Ji, Z.D. Wei, S.G. Chen, L. Li, J. Phys. Chem. C 113 (2009) 765–771.
[150] M. Mathias, J. Roth, B. Sompalli, M. Schoeneweiss, D. Wood, US2,004,137,311 (2004).
[151] J. St-Pierre, D.P. Wilkinson, S. Knights, M. Bos, J. New Mater. Electrochem. Syst. 3 (2000) 99–106.
[152] M.C. Johnson, D.P. Wilkinson, C.P. Asman, M.L. Bos, R.J. Potter, US5,840,438 (1998).
[153] M.S. Wilson, J.A. Valerio, S. Gottesfeld, Electrochim. Acta 40 (1995) 355–363.
[154] H.K. Atiyeh, K. Karan, B. Peppley, A. Phoenix, E. Halliop, J. Pharoah, J. Power Sources 170 (2007) 111–121.
[155] J. Chen, T. Matsuura, M. Hori, J. Power Sources 131 (2004) 155–161.
[156] F. Barbir, PEM Fuel Cells: Theory and Practice, Elsevier Academic Press, New York, 2005, pp. 163–186.
[157] X. Li, Principles of Fuel Cells, Taylor & Francis, New York, 2006, pp. 325–343.
[158] D.P. Wilkinson, O. Vanderleeden, in: W. Vielstich, H.A. Gasteiger, A. Lamm (Eds.), Handbook of Fuel Cells: Fundamentals, Technology and Applications, vol. 3, John Wiley & Sons Ltd., 2003, pp. 316–324.
[159] T.V. Nguyen, W. He, in: W. Vielstich, H.A. Gasteiger, A. Lamm (Eds.), Handbook of Fuel Cells: Fundamentals, Technology and Applications, vol. 3, John Wiley & Sons Ltd., 2003, pp. 325–336.
[160] X. Li, I. Sabir, J. Park, J. Power Sources 163 (2007) 933–942.
[161] S. Litster, J.G. Santiago, J. Power Sources 188 (2009) 82–88.
[162] J.S. Yi, J.D. Yang, C. King, AIChE J. 50 (2004) 2594–2603.
[163] A.P. Meyer, Glenn W. Scheffler, P.R. Margiott, US5,503,944 (1996).
[164] C.A. Reiser, WO9415377 (1994).
[165] C.A. Reiser, US5,700,595 (1997).
[166] S. Miachon, P. Aldebert, J. Power Sources 56 (1995) 31–36.
[167] S.H. Ge, X.G. Li, I.M. Hsing, J. Electrochem. Soc. 151 (2004) B523–B528.
[168] S.H. Ge, X.G. Li, I.M. Hsing, Electrochim. Acta 50 (2005) 1909–1916.
[169] T.A. Trabold, J.P. Owejan, US7,087,337 (2005).
[170] J.P. Owejan, T.A. Trabold, D.L. Jacobson, M. Arif, S.G. Kandlikar, Int. J. Hydrogen Energy 32 (2007) 4489–4502.
[171] G. Montie, R.B. Redlich, D.E. Leger, US20,080,213,648 (2008).
[172] M. Johnson, D.P. Wilkinson, J. Kenna, O.Vanderleeden, J. Zimmerman, M. Tabatabian, US6,586,128 (2003).
[173] T. Metz, N. Paust, C. Muller, R. Zengerle, P. Koltay, Sens. Actuators A 143 (2008) 49–57.
[174] T. Metz, J. Viertel, C. Muller, S. Kerzenmacher, N. Paust, R. Zengerle, P. Koltay, J. Micromech. Microeng. 18 (2008) 1–10.
[175] N. Akhtar, A. Qureshi, J. Scholta, C. Hartnig, M. Messerschmidt, W. Lehnert, Int. J. Hydrogen Energy 34 (2009) 3104–3111.
[176] T.V. Nguyen, US6,503,651 (2003).
[177] T.V. Nguyen, M.W. Knobbe, J. Power Sources 114 (2003) 70–79.
[178] M.W. Knobbe, W. He, P.Y. Chong, T.V. Nguyen, J. Power Sources 138 (2004) 94–100.
[179] T. Matsumoto, T. Tomizawa, K. Kokawa, T. Kanbara, S. Kobayashi, K. Hatoh, H. Kusakabe, H. Ohara, S. Takeguchi, S. Shibata, US2,004,224,206 (2004).
[180] D.P. Wilkinson, M. Blanco, H. Zhao, J. Wu, H. Wang, Electrochem. Solid-State Lett. 10 (2007) B155–B160.
[181] D.P. Wilkinson, R. Rahbari, J. Zimmerman, M. Blanco, US2,008,248,365 (2008).
[182] J.G. Santiago, J.D. Posner, F.B. Prinz, T. Fabian, J.K. Eaton, S.W. Cha, C.R. Buie, D. Kim, H. Tsuru, J. Sasahara, T. Kubota, Y. Saito, US2,006,029,851 (2006).
[183] T. Fabian, S. Litster, J.G. Santiago, C.R. Buie, H. Tsuru, J. Sasahara, T. Kubota, US2,007,284,253 (2007).
[184] C.R. Buie, J.D. Posner, T. Fabian, S.W. Cha, D. Kim, F.B. Prinz, J.K. Eaton, J.G. Santiago, J. Power Sources 161 (2006) 191–202.
[185] S. Litster, C.R. Buie, T. Fabian, J.K. Eaton, J.G. Santiago, J. Electrochem. Soc. 154 (2007) B1049–B1058.
[186] D.G. Strickland, S. Litster, J.G. Santiago, J. Power Sources 174 (2007) 272–281.
[187] K.Y. Ho, H.S. Han, S.Y. Kim, G.H. Rhee, J. Power Sources 185 (2008) 112–117.
[188] V. Palan, W.S. Shepard, K.A. Williams, J. Power Sources 161 (2006) 1116–1125.
[189] V. Palan, W.S. Shepard, J. Power Sources 159 (2006) 1061–1070.